UNITED STATES
NUCLEAR REGULATORY COMMISSION
WASHINGTON, D.C. 20555-0001

September 27, 2002

MEMORANDUM TO: John Zwolinski, Director
Division of Licensing Project Management
Office of Nuclear Reactor Regulation

FROM: Michael E. Mayfield, Director
Division of Engineering Technology
Office of Nuclear Regulatory Research

SUBJECT: EVALUATION OF REACTOR PRESSURE VESSEL NOZZLE TO HOT-LEG PIPING BIMETALLIC WELD JOINT INTEGRITY FOR THE V.C. SUMMER NUCLEAR POWER PLANT

Attached please find a letter report entitled, "Evaluation of Reactor Pressure Vessel Nozzle to Hot-Leg Piping Bimetallic Weld Joint Integrity for the V.C. Summer Nuclear Power Plant." This work was carried out by Battelle, Columbus. Publication of this report is a RES operating plan milestone under activity 1A1AAC associated with NRR user need NRR-2002-018. This document was reviewed by staff in EMCB/DE/NRR in August 2002. Since that time, the document has undergone revisions to implement the modifications identified by your staff and the reviewers in MEB/RES.

In this work, analyses were performed to determine detailed residual stresses in a bimetallic weld joint of the type used in the V.C. Summer plant's primary system piping to the reactor vessel nozzles. The entire history of fabrication of the weld joint was included in the analysis, including inconel Alloy82/182 buttering, post-weld heat treatment, Alloy 82/182 weld deposition, weld grind-out and repair, hydro-testing, service temperature heat-up, and finally service loads. Three sets of analyses were performed. These include: (i) analysis of a cold leg bimetallic weld used in an experiment conducted by Battelle in an earlier RES sponsored program, (ii) analysis of a typical design bimetallic weld in the V.C. Summer plant for the hot legs 'B' and 'C', and (iii) repair weld analyses of several typical repairs. The first analysis was performed to validate the analytical modeling developed under this work, while analysis (ii) was performed to predict the crack growth response within residual stress fields and operating loads for a typical hot leg plant weld. Assumed surface cracks (of different crack depths and lengths) that are oriented either axially or circumferentially in the bimetallic weld were analyzed. Analysis set (iii) quantified the important effect that weld repairs have on weld induced residual stresses and on the corresponding primary water stress corrosion (PWSCC) crack growth through the repair residual stress fields. Temperature-dependent tensile properties of Inconel 182 weld material were obtained for this work at Oak Ridge National Laboratory under RES support.

A qualitative comparison of the predicted residual stresses with the available measured data from the V.C. Summer's metallurgical examination report was encouraging. Additional measurement of through-thickness residual stresses in the bimetallic weld joints using a new deep-hole drilling procedure is recommended. A sensitivity study was performed to assess the

effect of the constants in the PWSCC crack growth equation on the predicted crack profiles for several time spans for assumed axial or circumferential cracks. A more detailed study could be performed in the future to define the PWSCC crack growth equation that is based on measured data.

If additional information is required, please contact Shah N. Malik (SNM) of my staff on 415-6007.

Attachments: As stated

effect of the constants in the PWSCC crack growth equation on the predicted crack profiles for several time spans for assumed axial or circumferential cracks. A more detailed study could be performed in the future to define the PWSCC crack growth equation that is based on measured data.

If additional information is required, please contact Shah N. Malik (SNM) of my staff on 415-6007.

Attachments: As stated

Distribution:
W. Bateman
T. Chan
W. Koo
M. Fields

MEB r/f

DOCUMENT NAME: g:\Malik\VC-Summer_Weld-Analysis-Report_NRR-Transmittal.wpd

OAR in ADAMS? (Y or N) Y ADAMS ACCESSION NO :_____ TEMPLATE NO. RES-006
Publicly Available? (Y or N) Y DATE OF RELEASE TO PUBLIC _____ SENSITIVE? N

To receive a copy of this document, indicate in the box: "C" = Copy without enclosures "E" = Copy with enclosures "N" = No copy

* See Previous Concurrence

OFFICE	MEB/DET		MEB/DET		MEB/DET		RES/DET	
NAME	S.N. Malik*		D.A. Jackson*		N. C. Chokshi		M. E. Mayfield	
DATE	9/27/02		9/27/02		9/21/02		9/27/02	

effect of the constants in the PWSCC crack growth equation on the predicted crack profiles for several time spans for assumed axial or circumferential cracks. A more detailed study could be performed in the future to define the PWSCC crack growth equation that is based on measured data.

If additional information is required, please contact Shah N. Malik (SNM) of my staff on 415-6007.

Attachments: As stated

Distribution:
W. Bateman
T. Chan
W. Koo
M. Fields

MEB r/f

DOCUMENT NAME: g:\Malik\VC-Summer_Weld-Analysis-Report_NRR-Transmittal.wpd

OAR in ADAMS? (Y or N) Y ADAMS ACCESSION NO.:_____ TEMPLATE NO RES-006
Publicly Available? (Y or N) Y DATE OF RELEASE TO PUBLIC _____ SENSITIVE? N

To receive a copy of this document, indicate in the box: "C" = Copy without enclosures "E" = Copy with enclosures "N" = No copy

*See Previous Concurrence

OFFICE	MEB/DET		MEB/DET		MEB/DET		RES/DET	
NAME	S.N. Malik*		D.A. Jackson*		N. C. Chokshi		M. E. Mayfield	
DATE	9/27/02		9/27/02		9/21/02		9/27/02	

Final Report

EVALUATION OF REACTOR PRESSURE VESSEL (RPV) NOZZLE TO HOT-LEG PIPING BIMETALLIC WELD JOINT INTEGRITY FOR THE V. C. SUMMER NUCLEAR POWER PLANT

Part of Task 8 of the BINP Program
(Contract Number – NRC-04-97-052, Job Code W6775)

September, 28, 2002

Prepared by Battelle
F. W. Brust, Y. P. Yang, P. M. Scott

SUMMARY

The purpose of this report is to study the cracking behavior in bimetallic welds of the type used in the VC Summer Nuclear power plant. Tensile weld residual stresses, in addition to service loads, contribute to PWSCC (Primary Water Stress Corrosion Cracking) crack growth. In October 2000 the V. C. Summer Plant was shut down for a normal refueling outage. During the normal inspection a leak was discovered in the vicinity and on an outlet nozzle to pipe weld for the hot leg pipe (large pipe from the reactor vessel to steam generator). Ultrasonic tests performed on the pipe from the inside surface revealed a single axial flaw near the top of the pipe. During destructive inspection of the crack zone, additional smaller axial flaws were identified, along with several small circumferential indications.

In order to be able to predict crack growth rates, and therefore, predict the amount of time required before leakage occurs in normal Pressurized Water Reactors (PWR), a detailed analytical model of the VC Summer bimetallic pipe weld was performed. All of the fabrication processes involved in the construction and repair of the VC Summer hot leg bi-metal weld were considered. This included hot leg buttering and welding of a pressure vessel nozzle to a stainless steel pipe using inconel 82/182 filler material, material removal and repair, heat treatment, and service loads. PWSCC crack growth predictions were made for the cases of weld residual stresses only, and residual stresses with service loads. Predictions of axial cracks growth rates along with circumferential crack growth rates were made. Some of the key results from this series of analyses are summarized in the following paragraphs.

For reducing the effect of both axial and circumferential PWSCC after weld repairs, inside welding followed by outside welding is preferred. Both cases were considered in the analyses since the precise repair sequence in the VC Summer plant was not known. This illustrates the power of computational weld models and suggests that field weld repairs should be designed and driven by a corresponding weld analysis to reduce the propensity for SCC in piping.

In particular, hoop residual stresses (which lead to axial cracking) after complete fabrication are mostly tensile in the weld region. For the case of outside weld repair followed by inside welding, high tensile residual stresses are produced everywhere. For the inside weld followed by outside weld case, a small zone of compressive hoop residual stresses develop at the pipe ID in the weld. Moreover, hydro testing does not alter fabrication residual stresses very much.

Service load effects on PWSC were also considered. Heating the hot leg pipe system up to operation temperature of 615 F actually reduces axial fabrication stresses to mainly compressive values due to the expansion of the hot leg pipe and the rigid constraint provided by the vessel and steam generator. Hoop residual stresses are unaffected by heating up to operating temperatures. Since as fabricated axial residual stresses are low at operating temperature, circumferential stress corrosion cracking is not expected due solely to fabrication stresses. Service loads dominate circumferential SCC.

Axial crack growth is dominated by fabrication residual stresses but the internal pressure does play an important role in PWSCC. Weld repairs can alter residual stresses in pipe fabrications.

In general, stress reversal in sign occurs near the start/stop locations of the repair. This can possibly result in a SCC crack stopper or slow down the crack growth rate as the crack approached these locations. A similar reversal in the sign of the stress occurs in a baseline weld near the torch start/stop locations or weld repairs.

The analysis results here show that axial cracking should be confined to the weld region. Starting from a crack 0.2 inches in depth, the crack should break through the pipe wall within two years. The crack nucleation time is something that should be studied in more detail in the future. Circumferential cracks should take about twice as long to become a through wall crack compared with axial cracks. Circumferential cracks will tend to grow longer than axial cracks. However, since service loads dominate circumferential cracks, they will slow their circumferential growth as they grow toward the bottom of the pipe. Here, by bottom of the pipe, it is understood to be the compressive bending stress region of the pipe. The service loads consist of thermal expansion mismatch, tension caused by 'end cap' pressure, and bending. The bending stresses caused by a bending moment are compressive 180 degrees from tension zone. Part through circumferential cracks that initiate in the tension zone and grow beyond the bending neutral axis may slow down as they approach the compressive bending stress zone. However, for non-fixed bending axes, where the tension zone changes, this may not be significant.

Grinding of welds may lead to scratches, which in turn may lead to crack initiation sites. Grinding of welds should be performed carefully. It is of use to study the effect of grinding on both residual stresses (caused by grinding) and crack initiation sites. Numerical models of the grinding process can and should be developed and used to guide field grinding operations.

Finally, PWSCC growth would be best considered using a risk based probabilistic approach using TRACLIFE or similar code because of the inherent variability in many factors that lead to corrosion cracking.

Final Report

EVALUATION OF REACTOR PRESSURE VESSEL (RPV) NOZZLE TO HOT-LEG PIPING BIMETALLIC WELD JOINT INTEGRITY FOR THE V. C. SUMMER NUCLEAR POWER PLANT

Part of Task 8 of the BINP Program
(Contract Number – NRC-04-97-052, Job Code W6775)

1.0 INTRODUCTION

In October 2000 the V. C. Summer Plant shut down for a normal refueling outage. During the normal inspection significant boron deposits were discovered in the vicinity and on an outlet nozzle to pipe weld for the hot leg pipe (large pipe from the reactor vessel to steam generator). Leakage records showed a nearly constant value of 0.3 GPM unidentified leakage from all sources, well below the plant technical specification limit of 1.0 GPM (see Reference [1]). The design geometry of the nozzle to pipe weld is shown in Figure 1. Ultrasonic tests performed on the pipe from the inside surface revealed a single axial flaw near the top of the pipe [1]. The flawed region was then removed, and a new spool piece was welded in place. The repair weld was made with Alloy 52, a material which is much more resistant to SCC (stress corrosion cracking) compared with Alloy 82/182.

The purpose of this report is to study the cracking behavior in bimetallic welds of the type used in the VC Summer plant. Tensile weld residual stresses, in addition to service loads, contribute to PWSCC (Primary Water SCC) crack growth. In order to be able to predict crack growth rates, and therefore, predict the amount of time required before leakage occurs in normal Pressurized Water Reactors (PWR), a detailed analytical model of the VC Summer bimetallic pipe weld was performed.

The work plan outlined here was to help support the NRC's assessment of the cracking found in the 'A' RPV nozzle to hot-leg pipe bimetal weld in the Virgil C. Summer nuclear plant. The hot leg weld is a bimetallic weld joining a SA-508 (Class 2) reactor vessel nozzle with a Type 304 stainless steel pipe using an Inconel weld procedure (Figure 1). Figure 2 illustrates the geometry of this type of nuclear plant in simple format. The hot leg pipe carries reactor-heated water to the steam generator. It is then re-circulated by the pump back through the 'cold leg'. Both the hot and cold leg stainless steel pipes are joined to the reactor vessel nozzles via bimetallic welds. The cracking of concern occurs in the Inconel weld only.

The analysis work reported here was broken into three tasks. The first task was to model the residual stresses that develop from welding. This analysis included the effects of selected repair weld analyses. The second was to validate the model by performing measurements on a similar bimetallic welded pipe that was obtained during an earlier NRC program at Battelle (Reference [2]). The final task involved evaluating stress intensity factors along with performing simple pressurized water stress corrosion cracking (PWSCC) analyses of the cracks. All work was performed as part of Task 8 of the BINP Program.

2.0 GENERAL OVERVIEW OF ANALYSIS WORK PERFORMED

Three separate sets of weld analyses were performed. These include: (i) analysis of a cold leg bimetallic weld used in an experiment conducted by Battelle in an earlier NRC sponsored program [2], (ii) analysis of a typical design bimetallic weld in the V. C. Summer plant for V. C. Summer hot legs 'B' and 'C', and (iii) Repair weld analyses of several typical repairs. The first analysis was planned for model validation purposes while (ii) was planned to predict the crack growth response within residual stress fields and operating loads for a typical hot leg plant weld. Analysis set (iii) quantified the important effect that weld repairs have on weld induced residual stresses and on the corresponding crack growth through the repair residual stress fields.

The analyses in sets (i) and (ii) were performed using both axis-symmetric analysis and full 3D analysis. The analysis set (iii) was performed using full 3D analysis. It is noted that 3D welding considerations can have an important effect on the residual stresses, especially in the region of the weld start/stop locations and for considering the effects of weld repairs. The axis-symmetric analyses of (i) and (ii) provided an initial 'general' overview of the residual stress fields in this bimetallic weld. However, as discussed below, full 3D effects will be included in the fracture assessment even for the axis-symmetric weld modeling case.

2.1 Weld Residual Stress Analysis

The series of weld modeling analyses listed below were performed.

- **Axis-symmetric Cold Leg Analysis.** A weld analysis of a bimetallic weld from a cold leg that was tested as part of the NRC program 'Short Cracks in Piping and Piping Welds' program was performed first. This pipe test was an A516 Grade 70 carbon steel pipe welded to a 316 SS safe end using an Inconel weld (Figure 3). The pipe diameter was 36-inch with a thickness of 3.4 inches. The materials and geometry of this case are similar to the hot and cold leg welds in the V. C. Summer plant. The purpose of this analysis was to validate the weld models for the bimetallic weld case. A length of cold leg pipe that was saved from an earlier program at the Battelle West Jefferson site was tested to obtain as welded residual stresses. It should be noted that Battelle's weld models (VFT^{TM} [3]) have extensive validation from other programs in industry, US Government, and overseas utilities. It will be seen, however, that the residual stress measurements results are in question.

- **Axis-symmetric Hot Leg Analysis.** Weld analysis of the design hot leg bimetallic welds in the V. C. Summer plant were conducted. This analysis was quite complicated since the actual field welds sequence; including grinding and repair were considered. This analysis predicted the residual stresses for use in a fracture assessment in Task 3. Weld joint specifications and material properties available from the licensee were provided by the NRC so as to accurately model the residual stresses.

- **Three Dimensional Analysis of Hot Leg.** The analyses discussed above assumed axis-symmetric conditions for the analysis. It is known that full three dimensional weld residual stress states can vary significantly from an axis-symmetric solution near the regions of the weld torch start/stop positions. In general, compressive residual stresses often develop near the regions of the start/stop locations. As such, an axis-symmetric solution is normally considered conservative compared with a full three dimensional solution. With this in mind, the three dimensional analysis of the hot leg weld was performed to quantify the '3-D' effect on PWSCC in PWR Two separate repair lengths and two depths (a total of three repair analyses) were performed. These consisted of a long and short length repair with a shallow depth, and a short length repair with a deeper depth. The repair solution procedure consists of first modeling the original bimetallic weld. This is a computationally intense solution since there are so many passes involved. Next, the material removal in preparation for the repair was modeled. Finally, the repair passes were modeled. For all repair cases, the predicted residual stresses were used to predict SCC crack growth.

Finally, all analyses will be performed using the VFT^{TM}'s weld analysis code (Reference [3]), which was developed jointly by Battelle and Caterpillar. This code has an extensive database of validation for complex welded structures and is considered to be the best available weld analysis code.

2.2 Weld Residual Stress Measurements

This task involved determining the residual stresses from the Battelle bimetallic test case to further validate the models for bimetallic welds. Battelle still has sections of the original pipes that were taken from a canceled plant, and several were tested (Reference [2]) but several sections still remain undamaged. A trepanning technique was used to obtain surface measurements of the residual stresses.

2.3 Fracture Mechanics and PWSCC Analysis

Stress intensity factors were determined by first mapping the results obtained from the weld analyses to a full three-dimensional finite element model. The stress intensity factors are determined from the residual stress fields using the finite element alternating method (FEAM) code developed by Battelle (Reference [4]). In addition, service loads were applied over top the residual stresses to obtain the loads for PWSCC analysis as well. FEAM is an extremely efficient method for fracture analysis that was developed recently in the aerospace community and has FAA and Air Force acceptance. In addition, Battelle has been using FEAM for weld fracture analyses for Argonne National Laboratory (as part of another NRC program), as part of a DOE weld fracture analysis program for Savannah River, and for European utilities. It is accepted as accurate and has been extensively validated. The effect of weld residual stress redistribution during crack growth is accurately accounted for with FEAM. The efficiency of FEAM is because a special crack mesh is not needed – rather the mesh for the *uncracked* geometry is all that is required, and K solutions can be obtained for many crack sizes, shapes, and locations with this one mesh.

Both circumferential and axial crack solutions were obtained for both surface and through-wall cracks. From the recent documentation of the V C Summer cracking it is clear that both types of cracking have been observed. Flaw indications have been identified using ultrasonic testing (UT) and eddy current testing (ECT) in hot legs A, B, and C as reported in 12/20/2000 and 01/18/2001 licensee public meeting presentations. K was determined for about 20 cracks of various sizes and locations. It is emphasized that the full 3D analysis using ABAQUS is time consuming and costly compared with FEAM solutions.

Finally, PWSCC predictions were made using the K solution results. The analyses of PWSCC include the effect of residual stress redistribution caused by crack growth. The TRACLIFE code (Reference [5]), originally developed for the FAA, was used to make the crack growth life predictions.

3.0 ANALYSIS TOOLS

From the discussion above, it is seen that three different analysis tools were used to perform these analyses. The analysis tools are:

1. VFT™ – Virtual Fabrication Technology and Weld Modeling Code.
2. FRAC@ALT - Finite Element Alternating Method (FEAM) Code.
3. TRACLIFE – Probabilistic and Deterministic Life Prediction Code.

Detailed discussion of each of these codes is supplied in the Appendices.

4.0 RESULTS COLD LEG ANALYSIS

As discussed above, the first step in the analysis of the hot leg PWSCC issue was to obtain confidence in the computational weld model. As discussed in Reference [3] and Appendix A, the VFT code used for the weld modeling analyses has an extensive validation data base library for same material welding (stresses and displacements). However, little data exists for bimetallic welds. As part of the validation of the analysis procedures for bimetallic welds, it was decided to perform a weld analysis of a cold leg pipe that Battelle had stored from the NRC Short Cracks in Piping and Piping Welds program (Reference [2]). This stored pipe then had its residual stresses measured using the classic trepanning technique (Reference [6]). The predicted residual stresses were then compared with the measured stresses. Unfortunately, the measured stresses appeared to be quite low compared with what was expected. This is discussed later in this section.

4.1 Cold Leg Computational Weld Model

Figure 3 illustrates the axis-symmetric weld model in the lower figure and a photograph of the weld cross-section for the bimetallic weld that was tested in the upper figure. It is seen that this pipe had A516 Grade 70 pressure vessel steel welded to a Type 316 stainless steel safe end pipe with Inconel 82/182 filler metal. Sixteen passes were required to complete the weld. This is a large diameter, thick pipe.

The analysis sequence flow chart is shown in Figure 4 and graphically illustrated in Figure 5. The A516 nozzle was first machined and a 304 stainless steel cladding was applied to the inner surface. The weld deposition of the 304 SS cladding layer was not modeled here. However, the material properties of the cladding were considered, i.e., a thin layer of 304 SS material properties was used at this region so that the material property mismatch is included in the inconel weld modeling steps. The weld cladding deposition step was not included here because cracking in the buttering and inconel weld metal was of main concern in this analysis. The residual stresses from the buttering, PWHT, and butt weld deposition will tend to dominate residual stresses in the region of interest (weld and butter zone). In effect, the local cladding residual stresses are 'annealed' or 'stress relieved' by the buttering and later weld processes and are of second order importance. Of course, such residual stresses are indeed important at regions away from the butt weld.

An Inconel buttering layer was then applied to the nozzle in preparation for the weld. From Figure 5 it is seen that the buttering was deposited in 11 passes. The nozzle was then subjected to a post weld heat treat of 1100 F for four hours. The post weld heat treat was modeled by permitting the stresses to relax via creep. The weld metal was then deposited to complete the bimetallic weld. Again from Figure 5, 16 passes were required. The buttering and weld sequence and weld pass sizes were estimated from the weld paper work for the actual production weld, and from the photograph of the weld cross section.

Figure 6 further illustrates the weld modeling process. It is also seen that the root pass was ground out after welding and re-deposited. It is not clear why this was done, but the process of grinding and re-welding the root pass was included in the model.

In modeling the weld process, particularly for multi-pass welds, it is important to properly model the history annihilation (or local 'annealing') process. Appendix A and the references illustrate this constitutive model and more details can be found in References [7, 8]. It is important to note that without modeling this history annihilation process, unrealistic plastic strains develop in the model predictions that have a significant effect on the predicted residual stress state. Moreover, the solution times of the computational model are significantly increased. The constitutive law is a classical thermal elastic-plastic law with features which permit history annihilation, phase changes (not important here), large deformations, melting/re-melting, and accounts for 'not yet deposited' weld metal in a computationally efficient manner using a concept called virtual element detection (Reference [8] and References cited in Appendix A).

The material properties used for the thermal analysis for the Inconel 82/182 weld metal, the A516 Grade 70 pressure vessel steel, and 316 and 309 stainless steels are shown in Tables 1 to 5. Tables 1 to 5 also list elastic properties used in the constitutive modeling of the weld process. Figure 7 illustrates the temperature dependent elastic plastic properties for the Inconel, A516 Grade 70, and Type 316 stainless steel used in the analyses. The tensile properties for Inconel 182 were obtained specifically for this program by Oak Ridge National Laboratory (ORNL). The elastic-plastic properties for the A516 Grade 70 were obtained from the literature, and the stainless steel properties were obtained from prior work done at Battelle. It is important to note that the thermo-plastic properties used for a proper weld modeling analysis (for the weld

material) should be stress relieved and annealed prior to testing since the weld modeling process itself models the work hardening process caused by the welding.

Finally, Table 6 shows creep properties used to model stress relaxation during the post weld heat treatment. Note that at 1100 F (the post weld heat treat temperature (PWHT)) the A516 Grade 70 steel experiences the most creep deformation. Moreover, note that the stainless steel (see Figure 5) is not in the model yet for the PWHT.

4.2 Cold Leg Results After Butter and PWHT

Figure 8 illustrates the axial residual stress state of the nozzle after buttering and PWHT is complete. (Note: all stresses in this report are in ksi units.) The analysis sequence begins in the upper left figure and proceeds clockwise. Note that by the time the PWHT is complete and cooling to room temperature occurs, the initial residual stress state has changed significantly. Likewise, the axis-symmetric hoop stresses through the PWHT process after buttering is shown in Figure 9. It is clear the hoop stresses are relaxed via PWHT more so than axial stresses. Moreover, including the effect of the PWHT in the analysis process is important.

The equivalent plastic strains after buttering and after PWHT are shown in Figure 10. It is noted that when modeling the PWHT process via a creep constitutive, plasticity is included (i.e., a combined creep-plasticity model was used). It is seen that the creep relaxation process is mainly due to creep, with additional plasticity having a second order effect. Figure 11 shows the effective creep strains that accumulate after the PWHT. The top illustration in Figure 11 is of a large portion of the nozzle. Notice the accumulation of creep strains near the end of the PWHT region (see Figure 5 also). Other researchers have observed this as well when modeling the heat treat process. Notice from the bottom illustration of Figure 11 that the largest tensile creep strains occur near the outer diameter of the A516 nozzle adjacent to the Inconel butter.

4.3 Cold Leg Results After Completed Weld

The axial residual stresses after completion of the weld are shown in Figure 12. The outline of the buttering and weld are shown in this figure outlined in white. The stresses start as tensile near the inner radius, become compressive in the mid thickness region of the pipe, and return to tensile near the outer surface of the pipe. This behavior is quite typical for same material welds in thick pipe (References [6] and [9]). Axial residual stresses at the cold leg operating temperature of 556 F are illustrated in Figure 13. The main difference between the room temperature (Figure 12) and operating stresses (Figure 13) are magnitude.

The hoop residual stresses at room temperature and operating temperature are shown in Figures 14 and 15, respectively. Notice that hoop residual stresses remain tensile through out the entire pipe thickness in the region of the weld for both temperatures. Again, this is quite typical for same material (i.e., non bimetallic) welds in both thick and thin pipe [6, 9]. Moreover, these higher hoop stresses and through thickness stresses favor axial crack growth via stress corrosion cracking mechanisms if entirely driven by residual stresses.

Figures 16 (a) and (b) show comparisons of axial weld residual stresses to measurements, while Figures 16 (c) and (d) show the corresponding hoop stress comparisons. The measurements were made at Battelle at our West Jefferson, Ohio site, where the cold leg pipe has been stored since 1988. The 'chip removal' or trepanning technique of Reference [6] (and many references sited therein) was used for the measurements. The trends for the axial residual stresses comparisons (Figure 16 (a) and (b)) are similar, but the measurements are lower than the predictions. The hoop residual stresses (Figures 16 (c) and (d)) measurements are quite low compared with predictions. Hoop residual stress measurements in bimetallic welds have not been reported in the literature as far as we can determine. However, from prior measurements and predictions of pipe (see References [6, 9] for same material welded pipe and many reference sited therein), hoop residual stresses are nearly always tensile and approaching yield, especially in the regions of the weld for both thick and thin pipe. The measured stresses here (Figure 16 (c) and (d)) are actually compressive in this region. This is considered unrealistic. Despite efforts to resolve this quandary, we could not identify errors in our measurement technique.

Therefore, the main purpose of this analysis effort for the cold leg, to validate the VFT weld modeling procedure for bimetallic welds, was not successful. However, the results are useful and provide insight for the hot leg analysis discussed next. When the residual stress measurements were obtained, and the low values were measured, the weld modeling procedure was completely re-evaluated. The post weld heat treatment was then considered in the analysis process. The weld processes and procedures for both the cold leg and hot leg were carefully re-evaluated. The material properties used for the weld analysis were carefully evaluated. In fact, a separate test program was initiated at Oak Ridge National Laboratory (ORNL) to obtain better temperature dependent material properties for inconel 182/82 weld metal and for A508 steel. It is important to recognize that the material properties of the weld material must be obtained on annealed weld samples because the weld modeling itself models the heating and cooling strain hardening explicitly. Hence, while the experimental residual stress measurements did not provide direct validation of the weld modeling, the insight that was obtained by considering all of the above processes was very important. Indeed, after all of these effects were considered, and re-analysis of the cold leg completed, the residual stresses predicted were lower than those originally predicted. However, they were still higher than the measurements. The fact that the hoop residual stresses measured at both the ID and OD are so low clearly indicates that the measurements were not accurate. Because the constraint in the weld direction (hoop direction) is high, as the weld bead cools, it shrinks and is constrained by the already cool material, producing high tensile residual stresses in all cases the present authors have seen in over twenty five years.

Measurement of residual stresses in bimetallic welds should be pursued in the future, perhaps using the new deep hole drilling procedures developed by Professor Smith of Bristol University (Reference [10]). Regarding the trepanning method of measuring residual stresses, it has served very well in past studies at Battelle in the late 1970's and should be regarded as a viable method for measuring residual stresses. However, it requires a skilled and experienced technician to carefully remove the pyramid shaped chips from the pipe.

Figure 17 illustrates equivalent plastic strains. Figure 18 shows the corresponding axial, hoop, and shear plastic strains after welding. It is interesting to note that the axial plastic strains are compressive for the most part in the buttering region while the hoop plastic strains are tensile

in the butter and weld. Moreover, from Figure 18 (c), rather large values of shear strain develop in the region of the butter. While PWSCC growth is considered to be driven by tensile stress, or stress intensity factors, it may be useful to consider the role of tensile plastic strains in SCC growth in future studies.

5.0 RESULTS HOT LEG ANALYSIS

This section presents the axis-symmetric results for the hot leg analysis. The results of this analysis were used to calculate stress intensity factors so that PWSCC predictions could be made (Section 6).

5.1 Hot Leg Computational Weld Model

The geometry of the hot leg bimetallic weld joint is illustrated in Figures 19 and 20. Note that the hot leg analysis for the VC Summer plant is similar to the cold leg analysis discussed in Section 4 except that the geometry is different (smaller diameter and thickness), and the materials are different for the nozzle (compare with Figure 3).

Please follow Figure 21 for the description of the weld modeling process. The modeling sequence is quite complicated since the VC Summer hot leg in question had several repairs made to it. The sequence of the repairs was not entirely known, so two repair sequences were considered. Figure 21 illustrates the welding sequence modeled. The nozzle was first pre-heated and a buttering layer deposited. The nozzle was then post weld heat treated (PWHT). As with the cold leg, the PWHT was modeled via creep analysis applied to the buttered weld residual stress state.

The buttered nozzle along with the stainless steel pipe was then pre-heated again and weld metal was deposited from the inside of the pipe to a depth of 0.7 inch. After this amount of weld metal was deposited, the weld was rejected. In preparation for weld grind out (of the original 0.7-inch of weld metal), a weld bridge was deposited. The weld was then ground out from the pipe inside. There were then two weld sequences that were considered in the analysis since it was uncertain whether the weld repair was deposited from the bridge first on the outside of the pipe, followed by the inner weld or vice-versa. Both were modeled to examine the effect of the repair sequencing on the final residual stress state.

All of the processes listed in Figure 21 were considered in the model. Figure 22 further illustrates the modeling process pictorially. Figure 22 (a) shows the original buttering model results. Figure 22 (b) shows the PWHT modeling process. Figure 22 (c) shows the completion of the weld prior to weld rejection, building of a weld bridge, and then grinding out the original weld so that only the bridge remains. Finally, the weld was either deposited from the ID first, then the OD, or vice-versa. Both were modeled since the precise repair weld deposition sequence was not known.

An important point regarding the analysis steps is in order at this point. Referring to Figures 21 to 23, grinding of weld material prior to deposition of the final weld passes was included in

the modeling process. For instance, from Figure 22 (c) to 22 (d), material was ground out to make a bridge of weld metal prior to deposition of the weld repair layers. This grinding process simply consisted of removing material 'computationally'. By this we mean that the material was removed mathematically by eliminating the stiffness of these elements and therefore redistributing the residual stresses. The actual grinding process, whereby a rigid (or nearly rigid) sharp tool impacted the weld region and material was 'chipped away' was not considered. This is a complex modeling problem, but it can be done. However, the main effect of the grinding is to redistribute the residual stress state in the pipe as material is removed and the precise modeling of the chipping process is not necessary.

There is another source of grinding that occurs after the entire weld repair is completed. Reference [12] provides summary of the metallurgical investigation of the cracking in the V. C. Summer plant. As discussed on page 9 of [12], 'The surface appeared highly irregular with evidence of significant surface grinding and machining distress marks'. Photographs and micrographs clearly show small 'scratch marks' along the inner pipe surface at the weld location (Figures 10 and 19 from Reference [12]). This grinding was presumably performed in order to remove the weld repair 'bulging' at the pipe ID in order to permit more uniform flow through the pipe. The grinding will redistribute residual stresses (as discussed above regarding the grinding before weld repair). However, because the material ground out is a small volume, it is not included in the analysis (i.e., the final geometry, already ground, is modeled).

In essence, if additional material was added to the ID weld, and then removed, the final residual stress state should be very similar to that from ignoring it except for very localized grinding stresses. The very local residual stresses from the grinding process are ignored in this case. Typically, additional residual stresses from grinding are considered to be important for only a very short depth into the thickness of the pipe. Certainly, after the crack grows a very short distance into the pipe thickness these local residual stresses are eliminated and the weld induced residual stresses dominate for most of the PWSCC growth life.

However, the geometric effects of the scratches are expected to be very important. These scratches should be considered as crack initiation sites for PWSCC, fatigue, or any possible cracking mode. Such grinding, which produces scratches, may serve as PWSCC initiation sites and should be avoided. It may be a useful exercise to include the actual modeling of grinding in such a model as an additional step in order to further prove this hypothesis. Moreover, since grinding is common practice, and is apparently not specifically considered by the code bodies, such a series of 'grinding' model studies may be of use in setting standards in future construction and aging repair.

5.2 Hot Leg Computational Weld Model – Buttering and PWHT Results

Figure 23 illustrates the entire analysis procedure for the hot leg. As seen, after the weld modeling is completed, results were mapped to a coarser two-dimensional model. The coarser two-dimensional model was then revolved to a three-dimensional model in preparation of the three dimensional PWSCC crack growth analysis. Service loads were then applied and crack

growth analyses were performed for the case of residual stress only and for residual stress with service loading. The crack growth portions of these analyses are discussed in Section 6.

The finite element model used for the analyses is shown in Figure 24. Note that the entire long length of pipe from the nozzle to the steam generator is included. It was originally thought that the long length of pipe could have an effect on the predicted weld residual stresses. However, two analyses were performed here: one with a free end (in the Type 304 SS length of pipe), and one with the length of pipe extending to the steam generator. It turns out that the weld residual stresses are not affected much by length of pipe. However, for the thermal loading (discussed next), it was important to include this length of pipe to accurately predict service axial stresses.

Figure 25 shows sequence plots of axial and hoop residual stresses after buttering and after post weld heat treatment. It is clearly seen that residual stresses are strongly affected by the PWHT. The hoop stresses are relaxed quite significantly. Figure 26 illustrates the equivalent plastic strains after buttering and after PWHT. After PWHT, plastic strains do increase somewhat more compared with the similar cold leg results (Figure 10). Corresponding creep strains after PWHT are illustrated in Figure 27. It is these creep strains that relax the weld induced residual stresses.

5.3 Hot Leg Computational Weld Model Results

Figure 28 (a) and (b) shows axial and hoop stresses after welding the first 0.7 inch depth weld on the inside of the pipe and after depositing the bridge layer. The bridge layer was apparently deposited to keep the pipes together during grinding and re-deposition of new weld passes. It is interesting to note that, due to global bending, compressive axial stresses (Figure 28 (a)) develop before removal of the material. Figure 28 (c) and (d) show the maximum and minimum principle stresses after removal of the weld metal with only the bridge material remaining.

Figure 29 shows axial and hoop residual stresses before repair (i.e., before grinding and re-deposition of weld metal) and after depositing the repair weld (inside weld repair case). Axial stresses actually reverse sign after the repair and the hoop stresses increase in magnitude after the inside repair.

Figure 30 shows axial residual stresses after the repair is complete. Two cases are shown: one where the inside welds is deposited first following repair, followed by the outer passes, and vice-versa. As discussed above, both cases are considered since the complete repair sequence is not known. The outline of the buttering layer and the weld material is shown for convenience. *It is important to note that axial residual stresses are more tensile, and cover a larger area at the inner surface of the pipe for the outside deposition first followed by inside welding.* This suggests that circumferential PWSCC (caused by axial stresses) is more likely for the outside weld first case. These results, and the model itself, can be used to define optimum weld sequencing for both repairs and for original welding. Figure 31 shows a similar comparison for hoop residual stresses for the two sequences. Again, the outside weld repair first case produces larger hoop residual stresses along the inner pipe surface compared with the inside weld first

case. Axial cracking is expected to be more severe for this case as well. This will be further shown in Section 6, which discusses PWSCC analyses.

Figures 32 through 35 provide comparisons of residual plastic strains caused by welding between the two sequences. In all cases except for shear strains (Figure 35), residual plastic strains are larger in magnitude, and cover a larger area for the outside weld first case.

Figure 36 shows the axial residual stress state after applying a hydro-test pressure at room temperature to the pipe over top the weld induced residual stresses. Hydro-test analysis assumes an end cap condition so axial stresses are applied as well as pressure. The hydro-test pressure was 1.4 times the PWR operating pressure of 2.25 ksi. The hydro-test does reduce the axial residual stresses somewhat. Figure 37 illustrates the effect of hydro testing on hoop residual stresses. It is seen that hoop residual stresses are not affected much by the hydro-test compared to the axial stresses.

As discussed in Section 4 regarding the cold leg analysis, the residual stress measurements performed using the trepanning method were somewhat disappointing. During the metallurgical investigation into the PWSCC cracking reported in Reference [12] residual stress measurements were made on sectioned pieces of the hot leg bimetallic pipe weld. Since the measurements were made on the pipe that was already cut up and sectioned, all component residual stresses are expected to be lower than in the intact pipe. However, from Table 2 of [12] the measured hoop residual stresses ranged from –8.6 to 23.4 ksi and the measured axial residual stresses ranged from 8.1 to 54.1 ksi. By comparing these numbers to the predicted residual stress plots in Figures 36 and 37 (after hydro-test and unloading) it is seen that the numbers are qualitatively similar. The hoop stresses measured from the cut pipe are expected to be most inaccurate since the weld bead (hoop) tension is relieved when the axial cuts are made to the pipe, and the hoop stress measurements are expected to be quite low. However, axial stresses are expected to be closer to the intact pipe. The ranges of measured axial stresses, when compared to Figure 36, compare reasonably well and provide some validity to the predictive methodology used here.

5.4 Hot Leg Computational Weld Model Results – With Operational Loads

The next step before calculating stress intensity factors for the PWSCC analyses is to obtain operating stresses. For the PWSCC analysis, we consider crack growth for both residual stress only and residual stresses with operational loading. The operational loading consists of temperature, which is 615 F, followed by a bending moment and pressure/tension load case.

The thermal loading was applied to the model of Figure 24. It was assumed that the entire hot leg was heated (and expands) to 615 F. The vessel and steam generator were assumed to be massive, providing the fixity constraints illustrated in Figure 24. Hence, the hot leg expands while the vessels provide constraint. Figure 38 compares the axial residual stress states before and after heat up to 615 F. The axial stresses decrease due to the hot leg expansion and vessel constraint. Figure 39 are the corresponding hoop residual stresses at 615 F. The small reduction in hoop stress is mainly due to the heat up (and corresponding reduction in material properties at high temperature). The constraint has little effect on the hoop stresses.

The detailed fine mesh required for the weld analysis is not required for the service load (moment and bending) case analyses. A fine mesh is also not required for the subsequent fracture analyses to be discussed next. As discussed in connection with Figure 23, the residual stresses are mapped from the fine weld (2D axis-symmetric) analysis model to a coarser (2D axis-symmetric) model. Figure 40 (a) and (b) provide axial and hoop residual stresses as mapped from the fine to coarse model. Figure 41 (a) and (b) provide the same mapping comparison for the outside first weld. It is seen that the mapping procedure is quite accurate.

Figure 42 shows a similar mapping between the coarse two-dimensional mesh to a full three-dimensional mesh. Again, the comparison is quite good (compare to Figure 41) illustrating that the mapping procedure is adequate. Figures 43 and 44 show similar comparisons between the 2D stresses and mapped 3D stresses. Finally, Figure 45 shows the plastic strains mapping from the coarse 2D mesh to the 3D mesh. This is explicitly shown to illustrate that stresses and strains are mapped to the three dimensional model. As such, the service load cases (moment, tension, and pressure) include the effects of plasticity.

6.0 PRIMARY WATER STRESS CORROSION CRACKING AND FRACTURE ASSESSMENT OF HOT LEG/RPV BIMETAL WELD

The finite element alternating method (FEAM) was used to obtain stress intensity factors to perform the PWSCC analyses. FEAM is very convenient for obtaining mixed mode stress intensity factors in complex structures. Stress intensity factors were obtained for numerous crack sizes and shapes for cases of:

- Inside weld first, then outside weld repairs
- Outside weld first, then inside weld repairs
- Residual stress only
- Residual stress plus normal operating loads
- Circumferential cracks
- Axial cracks

Typically it required about two minutes for a new solution on a high-end personal computer once the stiffness matrix was reduced once. Typical 3D meshes consisted of about 20,000 elements. In all, about sixty K solutions were obtained and used to model crack growth via SCC equations (discussed later). Although mode I stress intensity factors dominated, there were some cases where mode II was about 20% of the mode I value. However, mixed mode effects were not considered here.

FEAM properly accounts for stress redistribution as the cracks grow. As such, cracks that grow through a residual stress field that reach a compressive residual stress field (after stress re-distribution) can stop growing. Weight function methods often have problems accounting for stress redistributions properly. See Appendix B for details of FEAM and the FRAC@ALT code.

The results of the stress corrosion cracking assessment are provided here. For the SCC analyses, crack growth was predicted for the case of residual stress alone (at operating temperature of 615 F), and for normal operating loads. The normal operating loads were obtained from [11] and are included in Figure 46. The residual stress states that serve as input to the FEAM analysis are illustrated in Figure 47 to 50 for both the inside weld first case (Figures 47, 48) and outside weld first case (Figures 49 and 50). The top illustrations in Figure 47 to 50 consist of only the residual stress state at the operating temperature of 615 F. The bottom illustrations consist of residual stresses including operating loads. Plasticity (if any) was included in the analysis where loading was applied to the weld residual stress results.

Stress Intensity Factors. Figure 51 provides a few of the stress intensity factor plots used for the PWSCC assessment. This case is for an axial elliptic crack positioned with aspect ratio as shown in Figure 51. Both the 'residual stress only' and 'residual stress plus normal operating load' conditions were considered for all cases. In all K was calculated for cracks of many different sizes and shapes (a total of 60 cracks for both axial and circumferential locations).

The crack growth rate equation, taken from Reference [13], is:

$$\frac{da}{dt} = 1.4\times10^{-11}(K_I - 9)^{1\,16}(m/\sec) \qquad (1)$$

Here K_I is in MPa $m^{1/2}$ and the range for the data is for K between 20 and 45. The K values calculated in this study are both lower and higher than this value. Moreover, this equation represents the Scott model based on the application of a factor of 5. Hence, while this equation may need improvement for future analyses, it is used for the crack growth and life predictions shown in the following. Moreover, for this study, this was the only available data for the PWSCC crack growth analyses, i.e., no other PWSCC laws were used here.

6.1 The 3 Dimensional Growth of Axial Cracks Through the Hot Leg Weld

The growth of a 3 Dimensional (3D) crack through a thick pipe must account for both the residual stress field left from the welding process as well as the stress imposed from the applied loadings. Because the residual stresses can change from compressive to tensile (or vice versa) depending on the welding process, it is important to model the welding process as well as the pipe geometry and multi-axial loading.

For these analyses, two weld processes were studied. In the first, the weld was assumed to start from the inner diameter and proceed to the outer surface. This is denoted Inside-Out or I-O. The second was the reverse process, denoted Outside-In or O-I, where the weld was completed from the outside and then the inside weld was deposited. All results presented in Figures 52 through 55 use this designation in the description above the illustration. Using the results of the finite element analysis we can impose a residual stress field on the calculated results. Both I-O and O-I were considered since it is not known how the actual hot leg in the VC Summer plant was repair welded (see the discussion related to Figure 22).

Once the residual stress field has been calculated the applied loading is modeled, the FRACALT code (Appendix B) is used to determine the stress intensity factors, K, for a pre-defined set of crack sizes and orientations. These values of K are then normalized by $a^{1/2}$, where 'a' is the crack depth. We then sent the table of these normalized K values to the probabilistic mechanics code TRACLIFE (Appendix C) and calculated the crack surface changes during PWSCC growth using the above equation. For the purpose of this analysis, it was assumed that the value of K along the crack drove the growth and shape. TRACLIFE was selected for the analysis because it has already built into the program the necessary 3D calculation tools. In addition, it is possible to examine the impact of uncertainty on these calculations at a later time. The first case examined was the Inside-Out weld process. Because the residual stress field can lead to crack growth, **given that a crack exists**, we performed two sets of calculations. In the first, only the residual stresses were included. The second set of calculations added the applied loading. Note that the applied loading included the history of the entire weld process and plasticity was included in the analysis.

It is critical to remember that we are starting the calculations with an assumed crack depth of 0.20 inches. The question of initiation times and subsequent growth to the point at which the crack is 0.20 inches deep is completely ignored in these analyses. What we found was that there were relatively short growth times until the crack grows through the thickness. However, in addition to the two sources of uncertainty already mentioned, we have serious reservations about the stress-corrosion cracking growth model. The discussion sections will overview alternative ways to estimate the PWSCC crack growth law and the corresponding constants based on observed field crack growth data. However, it is what was available, so it was used.

Figure 52 (a-c) provides the results of these calculations. The axial cracks were introduced into the center of the weld. As discussed previously, there are numerous crack initiation sites provided by the grinding process of which any could begin to grow. In reality, the grinding scratch near the region of highest residual stress is expected to be the preferred dominant crack growth initiation site. Identification of the different plots is made as follows. In the legend above the plots, the curves are labeled as '3.0 Residual I-O' for instance (Figure 52 (a)). This represents the crack shape after 3.0 months of PWSCC with residual stresses only and welding from the inside first followed by completing the outside welds. The label '3.0 Load I-O' indicates the 3 month PWSCC crack shape for the case of load applied overtop the residual stress field (nonlinear analysis) for the I-O weld case.

The first thing of note is that the growth of the crack in the residual stress field without any applied loading is lower than when the load is applied. The plot shows the normalized (by the pipe thickness) crack depth. At the end of two years, with only the residual stresses, the crack is about 20 percent through the thickness. When the load is applied the crack is 95 percent through the thickness after one year. At about 14 months the crack becomes a through wall crack (TWC).

The small growth due solely to the residual stresses may seem like these residual stresses have little impact on PWSCC. However, if we perform an approximate analysis and assume that superposition applies in determining the stress intensity factors to use in the PWSCC equation, then we can estimate the impact of the residual stress field. For this we subtracted the stress

intensity factors for the residual stress fields only from the residual stress fields with loading applied. (Recall that the loads were applied on top of the residual stress fields and all history including plastic strains were accounted for.) Figure 52 (b) shows this calculation for a number of different times. As an example, after 12 months, the 'dark blue' curve represents the crack shape for the I-O weld for the case of residual stress and applied service loads. It is seen that the crack is approximately 95% through the pipe wall. The pink curve labeled '12 mo load only' crack shape for a load only case after 12 months of PWSCC, i.e., no residual stresses are included. This crack is about 32% through the pipe wall. The small light blue curve represents the crack shape for residual stress only after 12 months. This crack is only about 12% through the pipe wall. Hence, because the crack growth law is a nonlinear function of stress intensity factor, and additional plasticity occurs as the service loads are applied over top the weld residual stresses, the effect of the residual stresses on PWSCC is significant.

Finally, Figure 52 (c) shows the three and six month crack growth shapes for both the inside first weld followed by the outside weld (I-O) and the outside weld first, then inside weld (O-I) case. One can also compare the crack shape and depth for the residual stress only case and the residual stress plus load cases.

In Figure 53 is identical to Figure 52 (c) except shading is introduced to point out these effects. The 'red' shape represents the crack shape for the case of loading and residual stresses (for the I-O case) and the 'white' shape is the crack shape for the residual stress only case after 6 months of PWSCC growth. The 'red' curve (I-O case) can be compared to the 'gray' (O-I case) curve for a comparison of the weld sequence effect.

Figure 54 shows the circumferential crack growth shape after three and six months for the different cases. The O-I case tends to grow cracks wider than the corresponding I-O case while for the I-O case, the cracks grow somewhat deeper. This is expected by comparing the hoop residual stresses between the two analysis cases (Figures 43, 44, 48 and 50).

Equation (1), which was taken from Reference [13], was a fit to data the available test data (Figure 4-2 in [13]). The fit of the data was conservative and tends to represent an upper bound to PWSCC crack growth predictions. If we take that same data and provide a least squares regression fit to the data, we obtain the following:

$$\frac{da}{dt} = 2.16\times10^{-11}(K_I - 9)^{0.8} (m/\sec) \qquad (2)$$

Comparing Equations (1) and (2) one notices that the constant is larger and the exponent is smaller in (2). A comparison of predicted PWSCC crack growth using the less conservative regression fit (Equation (2)) to the original law is shown in Figure 55. Figure 55 (a) illustrates that an axial crack will break through the pipe wall sometime after 2 years using the regression fit compared to about 1 year using the conservative PWSCC rate curve. In Figure 55 (a) and 55 (b), the label '12.0 mo Regression Fit' represents the crack shape after 12 months of PWSCC growth using the Equation (2) regression fit while '12.0 Load O-I' is the crack shape using Equation (1). Similar notation is used for other times, i.e., '23.5 Load O-I' represents the

PWSCC crack shape after 23.5 months using Equation (1), etc. Figure 55 (b) indicates that the circumferential crack will break through the pipe wall at a time after 4 years using the regression PWSCC rate curve compared with about two years using the conservative PWSCC rate equation. This illustrates the importance of using a correct PWSCC law and the need for more PWSCC data. Moreover, from Figure 4-2 in [13], it is clear that significant scatter exists in the PWSCC test data. Because of this scatter, a risk based probabilistic assessment of PWSCC is in order.

6.2 The 3 Dimensional Growth of Circumferential Cracks Through the Hot Leg/RPV Nozzle Bimetal Weld

Axial crack growth in the hot leg/RPV nozzle bimetal weld is mainly driven by the hoop stresses, although stress redistribution during PWSCC crack growth through the pipe wall thickness is influenced slightly by other stress components. Figures 48 and 50 show the contour plots of hoop stresses (i) after welding and heating to 615 F and (ii) service loads applied to the (i) case.

Circumferential crack growth is mainly driven by the axial stresses. Referring to Figure 38, note that the tensile axial stresses at room temperature are nearly all reversed to compression in the weld region as the pipe system is heated to 615 F. The end conditions of the hot leg (reactor vessel and stream generator) are assumed fixed for the thermal analysis. As such, when the hot leg is heated up it is constrained from expansion at the ends. The residual stresses reduce to compression as seen in Figure 38. In contrast, the axial expansion of the hot leg has minimal effect on hoop stresses.

Referring to Figures 38, 47 and 49 compressive axial stresses exist in the pipe near the weld region for the case of no load except in a small region on the ID near the buttering region. Hence, circumferential crack growth *due solely to residual stresses (at 615 F operating temperature)* is not expected except for possible small growth at the ID near the butter region. The bottom illustrations in Figures 47 and 49 represent axial stresses with the loads (pressure, tension, and bending – see Figure 46) applied. The loads were applied to the initial conditions of residual stress state at 615 F. Very little additional plasticity occurred during application of the loads because the axial residual stress state is compressive before application of the load. For the hoop load case, because the initial hoop residual stresses are high before application of the load, plasticity during application of the pressure does occur. From Figures 47 and 49 it is clear that the applied loads would be the main contributor to circumferential crack growth in contrast to axial crack growth where the hoop residual stresses dominate crack growth.

The circumferential crack growth profiles for the I-O and O-I cases are shown in Figures 54a and 54b. The initial flaw size for this case is 0.2-inch also. Because the 3D model has a symmetry plane at the center of the elliptic cracks, only the crack shape from 0 to 90-degrees is shown. It is seen that crack growth favors a location at an angle away from the deepest point of the crack. This is somewhat typical for circumferential cracks in homogeneous materials [14]. It takes approximately 3 years for the crack to break through the pipe wall. The axial cracks grow about twice as fast.

The crack growth law shown in the above Equation was obtained from [13] and was necessarily conservative. If we make a regression fit of the PWSCC test data for Alloy 182 at 615 F (Figure 4-2 of Reference [13]), different growth response is obtained. Figure 55a and 55b compare axial and circumferential crack growth for different PWSCC growth laws. It is clearly seen that crack growth predictions depend strongly on the accuracy of the SCC data fit. The SCC predictions would be best interpreted using a probabilistic approach using TRACLIFE and this should be pursued.

7.0 THREE DIMENSIONAL WELD EFFECTS

As discussed in References [1, 11, 13], the bimetallic hot leg weld that experienced field cracking had a number of repairs done to it. Because repair welds are inherently three dimensional in nature, some limited analyses were performed in order to obtain a qualitative assessment of three-dimensional effects on the bimetallic weld and weld repair process.

Figure 56 illustrates the model that was considered. The butter layer, PWHT, and hydro-test were not considered, and the boundary conditions at the vessel and steam generator were not considered (i.e., the length of pipe shown in Figure 56 was modeled). All of the weld passes shown in Figure 20 were not considered. Rather, passes were lumped together to form 7 passes as shown in Figure 56. All of the conditions in Figure 23 could well have been considered but were neglected due to time constraints. In the future, it may be useful to perform complete 3D analyses of this pipe.

Figure 57 illustrates the repair cases considered: two different lengths and two different depths. All four analyses considered the baseline weld first followed by grinding and deposition of the repair weld passes. The definitions of the original weld and repair weld geometry convention are shown in Figure 58. The X = 0 location represented the start/stop positions of the baseline weld. The repair welds modeled ranged from A to B (Length L_2) and A to C (Length L_1) with the angular definitions shown in Figure 58. Figure 59 shows the analysis on the long (L_1) and deep (d_2) weld repair in progress.

Axial residual stresses for the baseline three-dimensional weld are shown in Figure 60. The section is at the center of the weld and includes the A508 nozzle. Notice that the axial stresses near the start location are different from a location far away from the start location where near steady state conditions exist. In essence, the axial stresses reverse sign compared with locations away from the start/stop location. This can actually help in slowing down circumferential SCC growth as the crack grows into this location. Figure 61 shows a similar axial stress plot for the baseline weld for a longitudinal cut section. Figure 62 shows a similar plot of Z-component stresses (see coordinate axis in Figure 62). It is also seen that compressive stresses develop near the start/stop location that can slow down longitudinal crack growth. However, this reduction in residual stress state must be balanced by the fact that start/stop locations are often regions where weld defects can occur. Note that the Z-component stresses represent hoop stresses on the cut planes.

Figure 63 compares weld residual stresses between the axis-symmetric and three-dimensional analyses at room temperature. Of course, the three-dimensional solution did not

include the butter step, the PWHT after buttering, and the passes were deposited in only seven passes. Despite these differences, the comparison of hoop stresses at a location far from the start/stop location is not entirely dissimilar. In general, the three dimensional solution predicts more compression in the weld at the ID compared with the axis-symmetric solution.

Figure 64 shows weld residual stresses after repair weld case 1 is complete. This is the case of the long, shallow weld repair (see definitions in Figure 58). Axial residual stresses reverse sign near the start and stop locations of the repair while stresses within the middle of the repair do not change much from the baseline steady state locations. Figure 65 shows a similar plot of axial stresses for a segment that consists of an angular cut of the weld repair. The effect of the repair on residual stresses is evident. Figures 66 and 67 show similar results for repair case for the short, shallow weld repair. Figure 67 is a plot of mean stress, which is a measure of constraint caused by welding and repair. It is seen that weld repair does induce significant constraint near the beginning and end points of the repair. Constraint can influence fracture response, and possibly SCC rates, but were not considered here since little work has been performed to date that investigates the effect of constraint on SCC rates.

Figures 68 and 69 show axial and mean stress for the short, deep weld repair. Comparing Figures 66 and 67 to Figures 68 and 69 shows that the compressive stress that develops near the beginning and end of the weld repairs is deeper for the deeper repair. This actually suggests that weld repairs may help slow down SCC growth and act as crack stoppers. Figure 70 provides a plot of equivalent plastic strain for the short, deep repair. It is clear that plastic strains increase along the entire length of the repair.

8.0 DISCUSSION AND CONCLUSIONS

Analyses of the residual stresses and PWSCC for the hot leg/RPV nozzle bimetal weld of the VC Summer plant were performed. The entire history of fabrication of the weld was included in the analysis, including inconel buttering, PWHT, weld deposition, weld grind-out and repair, hydro-testing, service temperature heat-up, and finally service loads. Some of the conclusions are described in the bullets below.

- An analysis of a cold leg pipe bimetal weld was performed first and residual stresses were measured from a bimetallic weld section that Battelle had secured earlier from a canceled plant. The measurements appeared rather low compared with what was expected. For instance, hoop stresses in the weld were compressive at both the ID and OD of the pipe. This does not appear reasonable based on experience. As such, additional measurements of bimetallic pipe welds should be made using a different measurement technique.

- To obtain a reasonable description of fabrication induced residual stresses, all of the fabrication steps should be considered in the analyses.

- The as fabricated *axial weld residual stresses* alternate sign as one proceeds from the ID to the OD of the pipe near the weld region. Tension to compression to tension back to compression axial residual stresses develop in the as fabricated pipe weld. The tensile stresses were highest at

the ID for the case of the outside weld repair deposited first and finishing with the inside weld compared with the opposite case.

- For reducing the effect of circumferential PWSCC after weld repairs, inside welding followed by outside welding is preferred.

- Final hoop residual stresses after complete fabrication are mostly tensile in the weld region. For the case of outside welding followed by inside welding after the bridge repair, high tensile residual stresses are produced everywhere. For the inside weld followed by outside weld case, a small zone of compressive hoop residual stresses develop at the pipe ID in the weld.

- Hydro testing does not alter fabrication residual stresses very much.

- Heating the hot leg pipe system up to operation temperature of 615 F reduces axial fabrication stresses to mainly compressive values due to the rigid constraint provided by the vessel and steam generator. Hoop residual stresses are unaffected by heating up to operating temperatures.

- Since as fabricated axial residual stresses are low at operating temperature, circumferential stress corrosion cracking is not expected due solely to fabrication stresses. Service loads dominate circumferential SCC.

- Axial crack growth is dominated by fabrication residual stresses.

- Weld repairs can alter residual stresses in pipe fabrications. In general, stress reversal in sign occurs near the start/stop locations of the repair. This can possibly result in a SCC crack stopper or slow down the crack growth. A similar reversal in the sign of the stress occurs in a baseline weld near the torch start/stop locations.

- Based on the PWSCC crack growth law from Reference [13] and the analysis results here, axial cracking should be confined to the weld region. Starting from a crack 0.2 inches in depth, the crack should break through the pipe wall within two years. The crack nucleation time is something that should be studied in more detail.

- Circumferential cracks should take about twice as long to become a through wall crack compared with axial cracks. Circumferential cracks will tend to grow longer than axial cracks. However, since service loads dominate circumferential cracks, they will slow their circumferential growth as they grow toward the bottom of the pipe. Here, by bottom of the pipe, it is understood to be the compressive bending stress region of the pipe. The service loads consist of thermal expansion mismatch, tension caused by 'end cap' pressure, and bending. The bending stresses caused by a bending moment are compressive 180 degrees from tension zone. Part through circumferential cracks that initiate in the tension zone and grow beyond the bending neutral axis may slow down as they approach the compressive bending stress zone. However, for non-fixed bending axes, where the tension zone changes, this may not be significant.

- PWSCC growth would be best considered using a risk based probabilistic approach using TRACLIFE.

- Weld repairs alter pipe residual stress fields near the start/stop regions of the repairs. This may help slow down a growing stress corrosion crack.

- Grinding of welds may lead to scratches, which in turn may lead to crack initiation sites. Grinding of welds should be performed carefully. It is of use to study the effect of grinding on both residual stresses (caused by grinding) and crack initiation sites. Numerical models of the grinding process can be developed.

9.0 REFERENCES

[1] McIlre, A. R., "PWR Materials Reliability Project Interim Alloy 600 Safety Assessments for US PWR Plants (MRP-44) – Part 1: Alloy 82/182 Pipe Butt Welds", EPRI Report, TP-1—1491, April, 2001.

[2] Scott, P. M., et al., "Fracture Evaluations of Fusion Line Cracks in Nuclear Pipe Bimetallic Welds", NUREG/CR-6297, January, 1995.

[3] VFT™ (Virtual Fabrication Technology Software), Version 1.3, Developed Jointly by Battelle and Caterpillar (Caterpillar owned), exclusively distributed by Battelle Columbus Ohio, and The Welding Institute (TWI) (via separate contract with Battelle), Cambridge, England.

[4] FRAC@ALT© (FRacture Analysis Code via ALTernating method), Version 2.0, January, 1999, Battelle Memorial Institute.

[5] TRACLIFE™, Probabilistic Life Prediction Code, R. E. Kurth, Battelle, 2001.

[6] Brust, F. W., Stonesifer, R., *Effects of Weld Parameters on Residual Stresses in BWR Piping Systems* EPRI NP-1743, Project 1174-1, 1981.

[7] Brust, F.W., Dong, P., and Zhang, J., 1997, "A Constitutive Model for Welding Process Simulation Using Finite Element Methods," *Advances in Computational Engineering Science,* Atluri, S.N., and Yagawa, G., eds., pp 51-56.

[8] F. W. Brust and M. F. Kanninen, "Analysis of Residual Stresses in Girth Welded Type 304-Stainless Pipes", *ASME Journal of Materials in Energy Systems*, Vol. 3, No. 3, 1981.

[9] Dong, P., and Brust, F. W. "Welding Residual Stresses and Effects on Fracture in Pressure Vessel and Piping Components: A Millennium Review and Beyond", Transactions of ASME, Journal Of Pressure Vessel Technology, Volume 122, No. 3, August 2000, pp329-339.

[10] Thomas, A., Ehrlich, R., Kingston, E., and Smith, D. J., "Measurement of Residual Stresses in Steel Nozzle Intersections Containing Repair Welds", in ASME PVP Volume PVP 434, *Computational Weld Mechanics, Constraint, and Weld Fracture*, Edited by F. W. Brust, August, 2002.

[11] Schmertz, J. C., Swamy, S. A., and Lee, Y. S., "Technical Justification For Eliminating Large Primare Loop Pipe Rupture As the Structural Design Basis for the Virgil C. Summer Nuclear Power Plant", Westinghouse Report, WCAP-13206, April, 1992.

[12] Rao, G. V., et al., "Metallurgical Investigation of Cracking in the Reactor Vessel Alpha Loop Hot Leg Nozzle to Pipe at the V. C. Summer Nuclear Generating Station", WCAP-15616, Westinghouse Electric Company, January 2001.

[13] Westinghouse Electric Co., "Integrity Evaluation for Future Operation Virgil C. Summer Nuclear Plant: Reactor Vessel Nozzle to Pipe Weld Regions", WCAP-15615, December 2000.

[14] F. W. Brust, P. Dong, J. Zhang, "Influence of Residual Stresses and Weld Repairs on Pipe Fracture", Approximate Methods in the Design and Analysis of Pressure Vessels and Piping Components, W. J. Bees, Ed., PVP-Vol. 347, pp. 173-191, 1997.

[15] J. Zhang, P. Dong, F. W. Brust, W. J. Shack, M. Mayfield, M. McNeil, "Modeling of Weld Residual Stresses in Core Shroud Structures", International Journal for Nuclear Engineering and Design, Volume 195, pp. 171-187, 2000.

[16] Brust, F. W., and Dong, P., "Welding Residual Stresses and Effects on Fracture in Pressure Vessel and Piping Components: A Millennium Review and Beyond", Transactions of ASME, Journal Of Pressure Vessel Technology, Volume 122, No. 3, August 2000, pp329-339.

Appendix A

VFT™ – Virtual Fabrication technology and Weld Modeling Code.

VFT™ MODELING OF SELECTED STRUCTURAL ASSEMBLAGES

Two tremendous advantages are obtained by developing fabrication solutions via the computer. First, designing the fabrication to minimize or control distortions can significantly reduce fabrication costs. Second, controlling the fabrication-induced residual stress state can significantly enhance the structure's service life. For distortion control, fabrication design via modeling can:

- eliminate the need for expensive distortion corrections
- reduce machining requirements
- minimize capital equipment costs
- improve quality
- permit pre-machining concepts to be used

Residual stress control via modeling can:

- Reduce weight
- Maximize fatigue performance
- Lead to quality enhancements
- Minimize costly service problems

VFT™ (Virtual Fabrication Technology – Fabrication and Weld Modeling Computer Tools) was specifically developed for this purpose. It is a sophisticated physics/mathematics based computer modeling software tool for use in optimizing and designing metal fabrication processes for industry. Representing the culmination of an extensive 5-year collaborative effort between Battelle and Caterpillar, VFT™ is a state-of-the-art cutting and welding simulation technology (see Reference [3]). VFT™ allows rapid solutions for large complex metallic structures containing both single- and multi-pass welds and allows the user to consider or input all critical variables. The heart of the moving arc model is a proprietary suite of thermal solutions and special material routines. The weld simulation models have been extensively validated using laboratory samples and actual production components. The following sub-sections give an overview of VFT™ and illustrations of its capabilities, and detail its use in performing the analyses in this report.

Process Modeling and VFT™. Over the past twenty-five years, computational simulations of industrial processes have been developed to improve product performance, optimize the fabrication process and reduce costly prototype requirements. Recently emerging technical journals (such as Reference [A-1]) are entirely devoted to process model development and are geared for industry engineers rather than an academic audience. Fabrication-induced distortions and residual stresses, from plate product through cutting to weld fabrication and final product, are major contributors to the total distortion of large fabricated structures. Although VFT focuses on the two most important and difficult processes of fabrication, namely cutting and welding, it is important to recall that the history of prior fabrication, such as plate rolling effects or forming, can be accounted for as "initial conditions" in a VFT simulation.

Experts throughout the world have studied simulating the weld process to predict residual stresses, distortion or microstructure. Many researchers have developed algorithms that predict residual stresses and distortion in simple three-dimensional "breakout" weld models. Industrial users, however, require highly capable technology that permits them to analyze complex structures. Figure A-1 shows the complexity of some structures analyzed with VFT™. They include fabrications involving more than fifty parts, joined together by arc welding with hundreds of meters of weld material. Accurate prediction of residual stress and distortion in the structure require consideration of all the prior stress histories in the cut parts, the manner in which the parts are put into the fixture and tacked, and the specific sequence of weld bead placement. The need for speed and accuracy in the models becomes especially significant when engineers begin to use the tool to control distortion through optimized weld sequencing, pre-camber, and thermal stretching.

VFT™ Development. Because VFT™ is proprietary, the publications detailing the models are not extensive. However, References [A-2 to A-5] describe some recent general applications of the models for both thick and thin plate and References [A-6 to A-10] describe details of the thermal and structural models. Finally, Reference [A-11] provides twelve additional publications that summarize different aspects of the VFT package for both thick and thin applications.

Figure A-2 helps to describe the weld simulation modules of VFT (the cutting modules are similar and partially overlap). To perform the analysis, the operator develops a mesh using a "hex" generator, either independently or from a solid model. A graphical user interface (GUI) is then used to set up the thermal and structural analysis files. The GUI permits easy definition of weld paths and sequences, including multiple passes. An uncoupled thermal solution and a structural numerical solution then produce the stresses and distortions. Numerous analysis features permit distortion and stress control including fixture modeling, pre-camber and pre-bend effects, thermal tensioning and sinks, pre-bending and rollers. A library of extensive full-scale experimental data has been developed over the last five years and has been used for model validation. Figure A-2 represents the analysis of a large boom type structure that required 15 fillet, 12 groove, and 11 lap welds for a total of 22 meters of weld material.

Thermal Model. The thermal model is novel and represents key enabling technology for weld and cut analyses. Based on analytical closed form solutions appropriately superposed, it is called CTSP (comprehensive thermal solution procedure). All weld features are permitted, including weld start/stop effects, multiple passes, arbitrary weld joint, base plate cutouts and holes, and trailing heat and cooling sources. The moving weld torch is permitted and has been found to be critical to obtaining correct solutions. The solution is extremely rapid (100 to 1000 times faster than a numerical equivalent) and can greatly reduce file space requirements. Numerical thermal solution is also possible with the use of a DFLUX routine that properly transfers heat from the torch to the work piece using a new 'modified Goldak' procedure. The speed and accuracy of CTSP is a key driver in permitting large-scale analyses to be performed in a reasonable amount of time. Figure A-3 illustrates the time savings that result with CTSP thermal solutions for a huge frame structure the size of a room. (In the in-progress analysis of Figure A-3, the current weld torch location is visible.) CTSP provides temperature versus time histories for each weld pass. The solution is independent of mesh refinement. File size is minimized since temperatures are only calculated at nodes that are affected, usually in the

vicinity of the weld. For the example of Figure A-3, the numerical solution requires a file size in the tens of GB, while the CTSP temperature file size is about 100 MB.

Structural Model. The structural portion of the modeling is performed using ABAQUS with a special USER material routine that properly accounts for weld modeling. VFT™ development included writing a new general constitutive model (UMAT-CAT), accurate for weld modeling, with features that include efficient handling of yet to be deposited material, history removal (as material is melted), melting/re-melting, thermo-elastic-plastic material behavior and hardening, and many other features. A new GUI and a series of utility routines such as UFIELD and U-MAP (Figure A-4) permit the thermal and structural analyses to be performed in a seamless manner. The analysis package is extremely rapid, permits analysis of complex structures, and has been extensively validated through full-scale tests.

Validation. An extensive library of tests has been compiled to validate the thermal model, distortion predictions, and residual stresses. The specimens range from simple 3D structures to the complex examples of Figure A-1. Figure A-5 illustrates distortion comparisons between prediction and experiment for the boom shown in Figure A-2. VFT™ analysis procedures have also been used in the nuclear industry to control residual stresses (eliminate cracking) and to examine crack opening shapes near weldments for leak-before-break considerations. It has also been used in steel frame construction, jet engines and the NASA space shuttle external tank, as well as for Navy tee stiffener applications and numerous automotive applications. Procedures to account for weld buckling for thin fabrications (less than 6 mm) were added to VFT™ for automotive frame distortion control applications.

Ship Structure Example

An illustration of the distortion control procedures for typical ship-type fabrications are found in Figure 6. The top portion of this figure compares VFT™'s distortion predictions to actual measurements for typical Tee beams. (Only a sample of a much larger series is presented in Figure 6.) A number of Tee beams of sizes and shapes typical of ship stiffener dimensions were modeled using VFT™. As shown in the diagram incorporated in Figure 6, they were joined using double sided welds where the weld was first finished along one side and then the other side was completed. After the predictions were made, weld experiments were performed. The table in Figure 6 illustrates the remarkable accuracy of the predictions.

More importantly, it is clear that weld parameters (e.g. heat input, torch speed, material) strongly affect the final distortion. The 40' by 80' hull assemblage in the bottom portion of Figure 6 was modeled for illustration using a typical welding sequence applied to 5 mm thick plate. The resulting distortions of the full structure illustrate the issues of concern, showing by comparison with the initial (undeformed) shape that the hull assemblage bows up along the long length. An assemblage like that in Figure 6, for example, will require ten to twenty separate analyses with varying parameters before the optimum sequence for distortion control can be realized.

References

[A-1] Computer Modeling and Simulation in Engineering, Ed. S. N. Atluri, *Sage Science Press*, Thousand Oaks California.

[A-2] Brust, F. W., et al., "Weld Process Modeling and Its Importance in a Manufacturing Environment", Society of Automotive Engineers (SAE) Technical Paper Series, Paper No. 981510, Warrendale PA, 1998.

[A-3] P. Dong, J. Zhang, Y. P. Yang, F. W. Brust, and J. K. Hong, "Advanced Weld Modeling Techniques and Applications in Design and Manufacturing of Automotive Structures," SAE Technical Paper Series No. 982364, Vol. 5, Body Manufacturing, Assembly, and Advanced Manufacturing, pp. 203- 209, (IBEC), Sep. 29 - Oct. 1, 1998, Detroit. MI, SAE International, Warrendale, PA, 1998.

[A-4] Brust, F. W., "Fabrication Optimization and Cost Savings Using Advanced Weld Modeling Tools", Invited presentation at 2001 American Welding Society (AWS) conference and expedition, Cleveland, OH, May, 2001.

[A-5] Brust, F. W., et al, "Advantages of Computer Based Weld Modeling In a Manufacturing Environment", Invited Paper, 2000 American Welding Society Conference, April, 2000, Chicago, Ill.

[A-6] Z. Cao et al., "A Comprehensive Thermal Solution Procedures for Multiple Pass and Curved welds", 2000 ASME Pressure Vessels and Piping Conference, Seattle, Washington, July 23-27,2000.

[A-7] Z. N. Cao, "An Efficient Heat-Flow Solution Procedure for Complex Welded Structures", 78th American Welding Society Annual Meeting, Los Angeles, April 13-17, 1997.

[A-8] Cao, Z. N., Brust, F. W., and Dong, P., "A Heat-Flow Solution With Convective Boundaries", Modeling and Simulation Based Engineering, Vol. II, Edited by Atluri and O'Donoghue, Technical Science Press, pp. 1732-1737, 1998.

[A-9] Cao, Z. Brust, F. W., Nanjundan, A., Dong, Y., and Jutla, T., "A Comprehensive Thermal Solution Procedure for Different Weld Joints", Advances in Computational Engineering and Sciences; ed. S. N. Atluri and F. W. Brust, Tech Science Press, pp 630-636, August, 2000.

[A-10] Brust, F. W., Dong, P., and Zhang, J., 1997, "A Constitutive Model for Welding Process Simulation Using Finite Element Methods," *Advances in Computational Engineering Science,* Atluri, S. N., and Yagawa, G., eds., pp 51-56.

[A-11] Brust, F. W., Jutla, T., Yang, Y., Cao, Z., Dong, Y., Nanjundan, A., et al, *Advances in Computational Engineering and Sciences; ed. S. N. Atluri and F. W. Brust,* Tech Science Press, pp 630-636, August, 2000. Numerous Weld Papers in this set of volumes on Weld modeling by these authors.

[A-12] Brust, F. W., Yang, Y., Dong, Y., and T. Jutla, "Weld Process Modeling and its Importance in a Manufacturing Environment", *Advances in Computational Engineering and Sciences; ed. S. N. Atluri and F. W. Brust*, Tech Science Press, pp 630-636, August, 2000.

Figure A-1. Examples of Complicated Structures Analyzed with VFT™

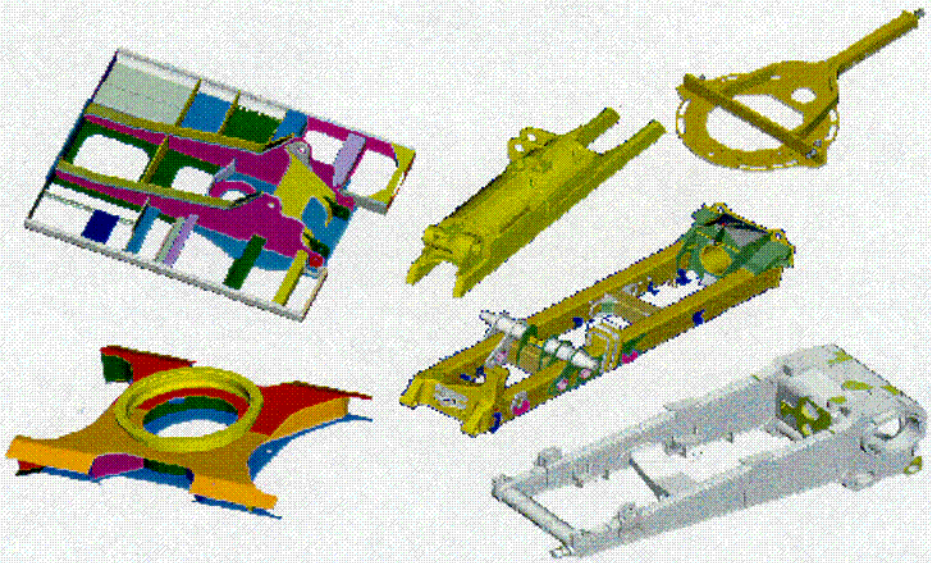

Figure A-2. Illustration of VFT™ Analysis Model for Welding

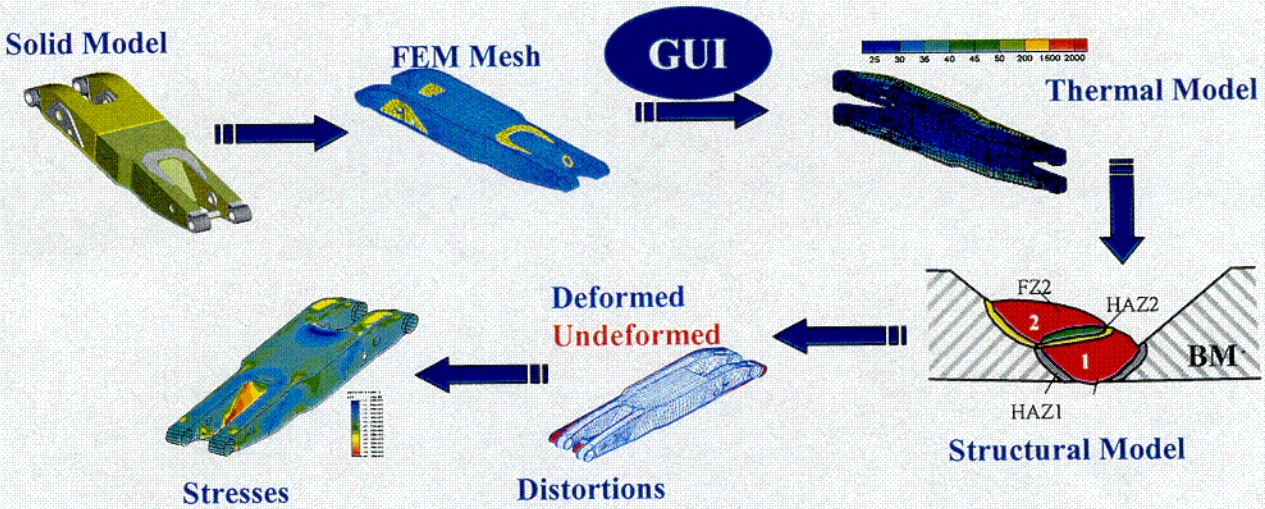

Figure A-3. Example computer timesavings with CTSP on huge frame

FEM: 240 hours
CTSP : 2.5 hours

Mesh: solid
Nodes: 52K
Elements: 37K
Frame Size: 5m x 5m

C01

Figure A-4. USER Routine Structure of UMAT-CAT Version 3.1.

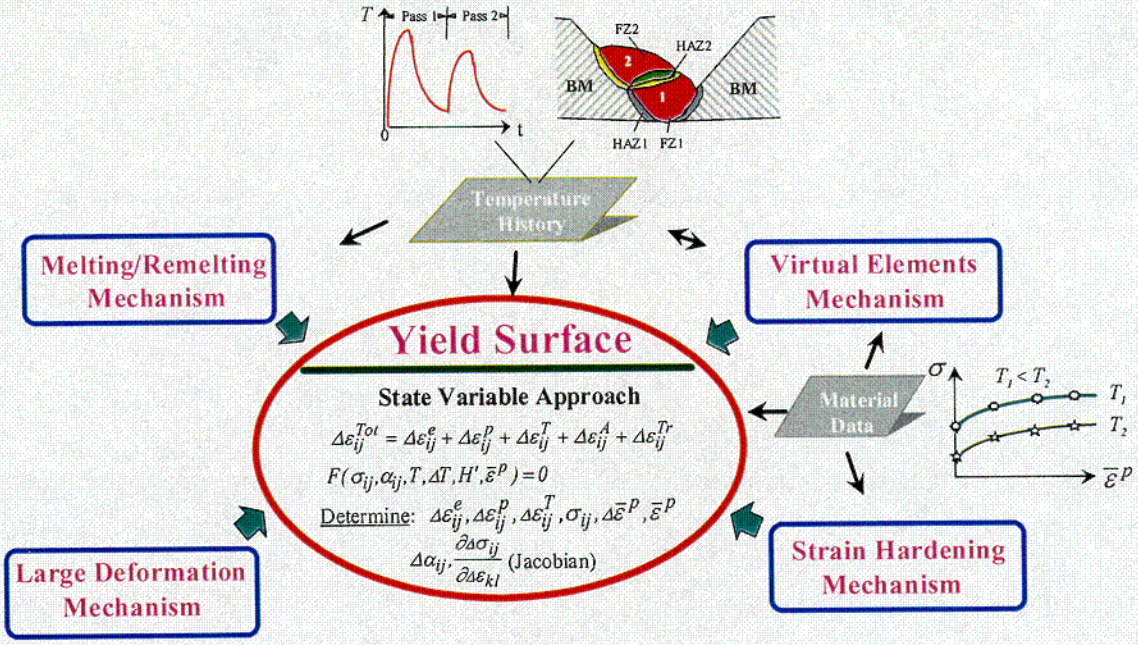

Figure A-5. Validation Problem for Boom – 22 piece parts.

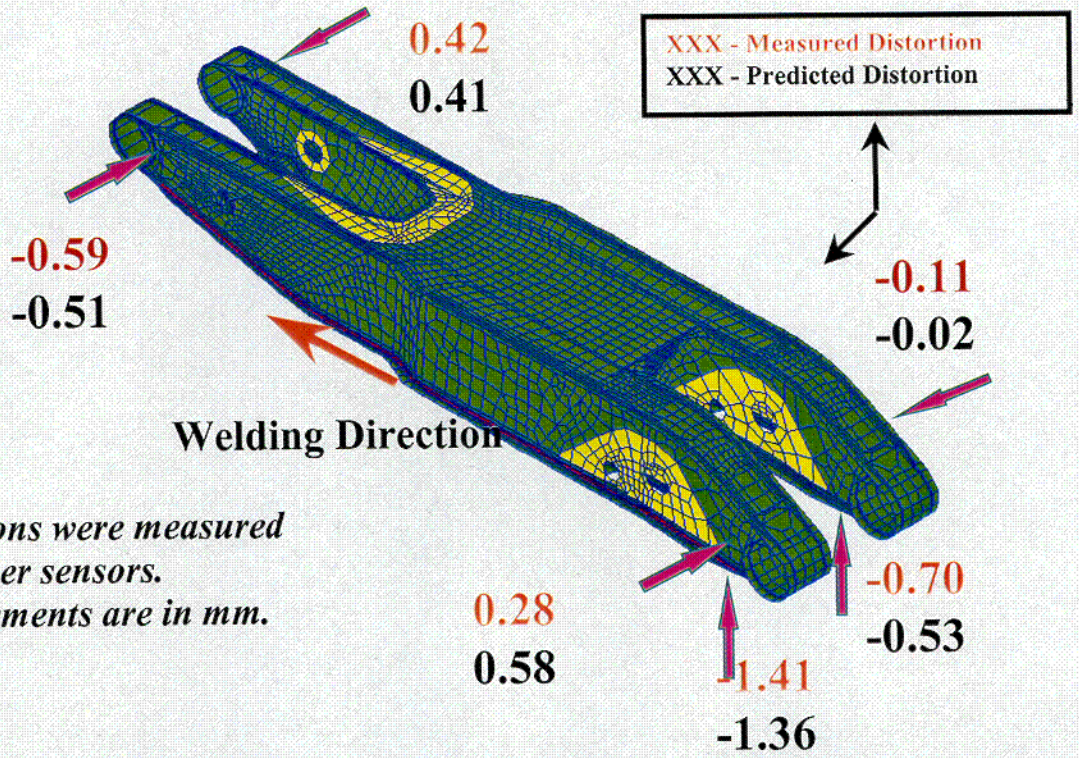

- *Distortions were measured using laser sensors.*
- *Measurements are in mm.*

C02

Figure A-6 Example Predictions of Typical Tee Beams and hull Assemblage (below).

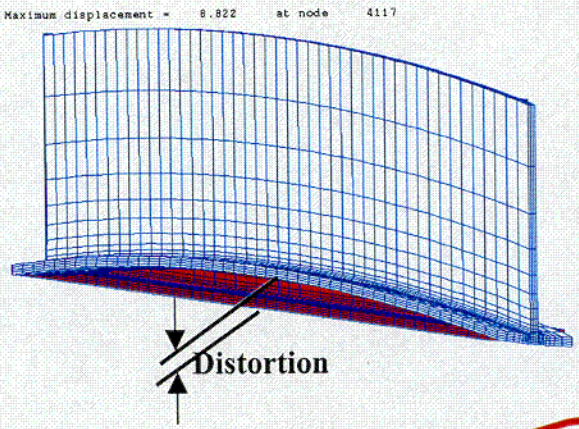

Mat-erial	Heat Input (kJ/mm)	Measured Distortion (mm)	VFT™ Prediction
A36*	O.8	6.1	6.0
A36*	1.4	9.5	8.8
HSLA-100*	0.43	1.3	1.5

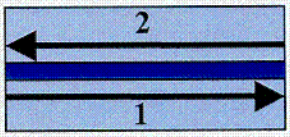

C03

Appendix B

FRAC@ALT and the Finite Element Alternating Method

THE FINITE ELEMENT ALTERNATING (FEAM) METHOD

The finite element alternating method (Reference [4]) is used in this report to obtain stress intensity factors for cracks that exist in weld induced residual stress fields. Here we provide a brief introduction to the method. The user is referred to the references for more details.

The fundamental mathematical concept of the alternating method has been known for more than one-hundred years. The method is quite general in that it can be applied to a wide range of elasticity problems. Scwartz (Reference [B-1]) treatment of the Dirichlet problem for two overlapping domains (or geometry's) involves using known solutions for two separate geometry's to obtain the solution for the more complex geometry obtained by partially overlaying the two regions. One may consider this as the solution for the union of the two original regions and the overlay region. Neumann [B-2] modified this concept to obtain the solutions for the intersection of the two geometry's. Neumann's observation is particularly useful since one of the domains can be an infinite domain where many closed form solutions exist. Since the method is applicable for any number of component geometry's, one can obtain the solution for doubly connected domains by using the solution for one infinite domain and one finite domain to obtain the solution to the doubly connected domain represented by the intersection of the two overlaid domains. With the finite element alternating method, the solution for a crack in an infinite solid loaded via arbitrary crack face traction's serves as the infinite domain solution while the finite domain solution is represented by the finite element portion of the solution. This is the source of the name Schwartz-Neumann finite element alternating method. It is noted that most current applications of the alternating method are for solving crack problems, although other difficult problems could be considered as well.

The current finite element alternating method (FEAM), which is summarized in References [A-3 to A-7], is the state of the art method for obtaining stress intensity factors for three dimensional surface and embedded crack problems and for two dimensional problems. Early versions of the method emerged in the late 1960's through the work of Kobayashi and co-workers [A-8]. However, the method was somewhat limited because the analytic solution was incomplete until Vijayakumar and Atluri [A-9] developed the complete solution for an elliptic crack in an infinite solid subjected to *arbitrary order surface traction's.* During the last eight years the method has been completely accepted as a practical computational tool to investigate fatigue and fracture problems in industry. The method has recently been extended to handle two and three-dimensional elastic-plastic and creep problems where the J-Integral and other fracture parameters may be evaluated for both stationary and growing cracks.

Figure B-1 schematically illustrates the FEAM method. These Figures illustrate the simpler 2D case for a crack in a weld. The infinite domain solution is actually the complete closed form solution for an elliptic crack in an infinite solid subjected to arbitrary order surface polynomials. The major advantage of the method, as seen in Figure B-1, is that a finite element mesh of *the uncracked geometry* is all that is needed to obtain stress intensity factors or the J-Integral (for plasticity problems, see References [A-10 to A-12]), displacements, stresses, etc. As seen in Figure1, the solution alternates between the infinite body closed form solution and the finite element solution for the finite body. Typically, 3 to 4 iterations are required. The mixed mode stress intensity factors are obtained naturally from this procedure.

The most important aspect of FEAM is that the same mesh can be used to obtain solutions for many different crack sizes, locations, and for multiple cracks. Because the finite element stiffness matrix only needs to be reduced once regardless of the crack size, crack

location, crack orientation, crack number (mixed mode conditions can be handled as well), etc., the method is extremely efficient.

For the K-solutions reported here, it typically took about 2 minutes to obtain solutions of K for the cases studied.

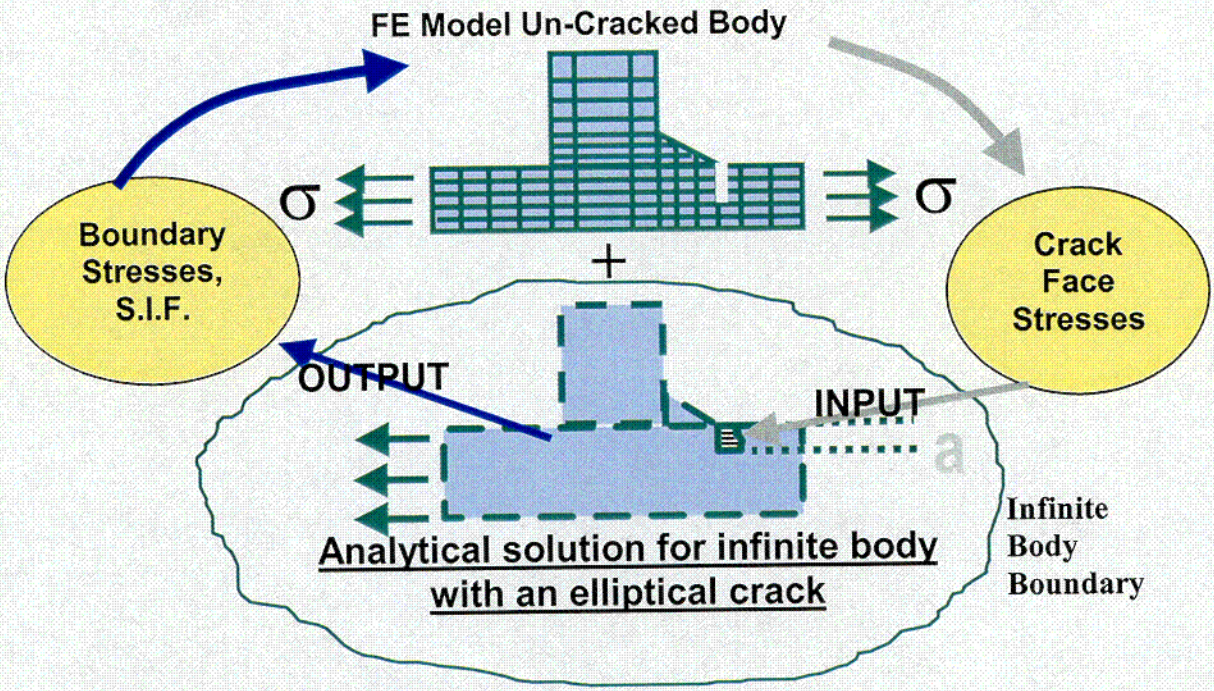

Figure B-1. Illustration of finite element alternating method.

References

[A-1] Schwarz, H. A., "Gesammelte Mathematische Abhandlungen", Vol. 2, pp. 133-143, circa 1865.

[A-2] Neumann, C., "Zur Theorie des Logarithmischen and Newtonschen Potentials", Leipziger Berichte, vol. 22, pp. 264-321, 1870.

[A-3] Nishioka, T. And Atluri, S. N., Analytical Solutions for Embedded Elliptical Cracks, and Finite Element Alternating Method for Elliptical Surface Cracks, Subjected to

C04

Arbitrary Loadings,□ Engineering Fracture Mechanics, Vol. 17, No. 3, pp. 247-268, 1983.

[A-4] Stonesifer, R. B., Brust, F. W., and Leis, B. N., □Mixed-Mode Stress Intensity Factors for Interacting Semi-Elliptical Surface Cracks in a Plate,□ Engineering Fracture Mechanics, Vol. 45, No. 3, pp. 357-380, 1993.

[A-5] Stonesifer, R. B., Brust, F. W., and Leis, B. N., □Stress Intensity Factors for Long Axial OD Surface Cracks in Large *R/t* Pipes,□ ASTM STP 1131, pp. 29-45, 1992.

[A-6] Nishioka, T. And Atluri, S. N., □Analysis of Surface Flaw in Pressure Vessels by a new 3 Dimensional Alternating Method,□ Journal of Pressure Vessel Technology, Vol. 104, pp. 299-307, November 1982.

[A-7] Atluri, S.N., □Energetic Approaches and Path Independent Integrals in Fracture□, Mechanics, in Computational Methods in the *Mechanics of Fracture edt. By S. N. Atluri,* North-Holland, 1986.

[A-8] Shah, R. C., and Kobayashi, A. S., "Stress Intensity Factor for an Elliptical Crack Under Arbitrary Normal Loading", Engineering Fracture Mechanics, Vol. 3, pp. 71-96, 1971.

[A-9] Vijayakumar, K., and Atluri, S. N., "An Embedded Elliptical Crack, in an Infinite Solid, Subject to Arbitrary Crack-Face Traction's", Journal of Applied Mechanics, Vol. 103, No. 1, pp. 88-96, 1981.

[A-10] Wang, L., Brust, F. W., and Atluri, S. N. (1995a), □Elastic-Plastic Finite Element Alternating Method and Prediction of Fracture, Part 1: EPFEAM Theory,□ to appear in Engineering Fracture Mechanics, 1996.

[A-11] Wang, L., Brust, F. W., and Atluri, S. N. (1995b), □Elastic-Plastic Finite Element Alternating Method and Prediction of Fracture, Part 2: Fracture and the T* Integral Parameter,□ to appear in Engineering Fracture Mechanics, 1996.

[A-12] Wang, L., Brust, F. W., and Atluri (1995c), □Elastic-Plastic Finite Element Alternating Method and Prediction of Fracture, Part 3: Application Prediction of the NIST Multiple Site Damage Experiments,□ to appear in Engineering Fracture Mechanics, 1996.

Appendix C

TRACLIFE CODE

METHODS USED FOR ANALYSIS

A computer program referred to as TRACLIFE was developed to assess all of the issues of concern in aging engineering systems. It was originally developed for the aircraft community with application to aging aircraft but was subsequently extended to permit analysis of diverse engineering systems, including aging nuclear plant components. More details of TRACLIFE are provided in References [1] and [2] and the references provided therein. In essence, TRACLIFE integrates methodologies developed in many different sources into a single probabilistic analysis procedure. TRACLIFE is a powerful tool for assessing a variety of factors on the overall risk of engineering structures in operation under the conditions of aging. A variety of conditions have been used in the engineering community to describe aging. Some of the damage mechanisms that can be addressed with TRACLIFE are:

- Crack initiation
- Linear and non-linear curved panel stress analyses
- Fatigue Crack growth
- Corrosion
- Corrosion fatigue
- Non-destructive Inspections
- Residual strength analyses
- Elastic-plastic fracture analysis
- Mixed mode fracture
- Multi-Site Damage (MSD)
- Multi-Element Damage (MED)

Clearly, the ranges of damage mechanisms that can be considered with TRACLIFE go well beyond what has classically been referred to as aging. The use of the computer program has been divided into two phases. The first phase of the analysis for a particular structure is deterministic, wherein the nominal behavior is calculated, in terms of local damage conditions, stress concentrations and crack driving forces. The second phase of the analysis involves the probabilistic modeling of the mechanics models, loads, and inspection procedures. The application in this report uses TRACLIFE to predict PWSCC crack growth without consideration of probabilistic aspects of damage.

Probabilistic Methods and TRACLIFE. The TRACLIFE code merges the deterministic methods discussed in the previous sections with the probabilistic methods illustrated in this section. The analysis procedure using TRACLIFE is also discussed. The major steps in designing a cradle to grave analysis of an aging structure are:

- Define the geometry
- Define the initial damage condition
- Define the fatigue crack growth model
- Define whether corrosion will be considered
- Select the residual strength model
- Set inspection intervals at selected time intervals or based on specified risk conditions

Each of these steps is complex. It is not possible to define a widespread fatigue damage analysis of an aircraft without having a working knowledge of structural mechanics. However, TRACLIFE does allow for an easy analysis of the *risk* factors associated with an aging aircraft once a consistent mechanics model has been developed.

TRACLIFE can use results from a number of finite element codes as input, including ABAQUS, ANSYS, STAGS, FRAC@ALT. The FEAM (for this application) code allows cracks to be inserted anywhere in the local model. This is critical for subsequent probabilistic fatigue and fracture analyses. More details of the stress analysis procedures were discussed above and in References [1, 2].

The available probabilistic methodologies include Monte Carlo, discrete probability distribution methods [21] (DPD) developed for NASA Johnson Space Center [22], PROF developed for the USAF [23], and Level II reliability [24]. The primary probabilistic engine is the DPD method, however, each is used as appropriate for efficient calculations. For example, the residual strength calculation is performed exclusively with level II methods. No further discussion of these methods is given here, other than to state they have been optimized to perform the calculations in fewer than four hours on a high end PC.

The results of the STAGS analyses are integrated into the TRACLIFE analysis in several ways. First, stress concentrations can be used to identify initiation sites. The local crack driving force, usually defined by the mode I stress intensity factor, K_I, is also developed via this analysis. The residual strength of the structure is subsequently calculated using the STAGS/FEAM analysis. Finally, a coupling of the probabilistic fatigue crack growth analysis and the residual strength analysis leads to a determination of the likelihood of the onset of aging issues.

References

[C-1] Kurth, R. E., and Bigelow, C., "Transport Risk Assessment Containing Widespread Fatigue Damage: TRACWFD Analysis of Longitudinal and Circumferential Splice Joints to Determine the Onset of Widespread Fatigue Damage and its Probability of Occurance", proceedings of the Joint Air Force, NASA, DOD Conference on Aging Aircraft, Williamsburg, VA, August, 1998.

[C-2] Brust, F. W., and Kurth, R. E., "Assessment of Analysis Methodologies for Predicting Fatigue Crack Growth and Residual Strength of Aging Aircraft", Proceedings of the 1997 Aircraft Structural Integrity Program Conference, Dec. 2-4, 1997, San Antonio, TX.

[C-3] Kurth, R.E., and Cox, D.C., *An Investigation of Discrete Probability Distributions for Probabilistic Fracture Mechanics Analysis*, Risk Analysis: An International Journal, 5, No. 3, 1985.

[C-4] Kurth, R.E. and Woods, K.S., *Probabilistic Damage Tolerant Analysis to Improve Aging Aircraft Maintenance and Inspection Schedules*, Invited paper, 1994 ASME International Mechanical Engineering Congress and Exposition, November 6-11, 1994, Chicago IL

[C-5] Berens, A.P. (1989), *Risk Analysis for Aging Aircraft Fleets; Task 1 Interim Report*, University of Dayton Research Institute Report UDR-TR-89-09.

[C-6] Hopkins, D.A., Chamis, C.C., *Probabilistic Structural Analysis methods: SSME Propulsion Components*, Advanced Earth-to-Orbit Propulsion Technology, 1, NASA Conference Publication 2436, 1986

Table 1 Material properties for INCONEL 182 weld material

T	C_p	λ	E	ν	σ_y	α
(°F)	(BTU/Lbm-F)	(BTU/Sec-inch-F)	(ksi)		(ksi)	(10^{-6}/°F)
70	0.095	0.00013	22674.70	0.3	38.50	6.50
200	0.110	0.000145	22023.96	0.3	36.18	6.73
400	0.120	0.000162	21022.83	0.3	33.55	7.09
600	0.125	0.000185	20021.70	0.3	30.00	7.44
800	0.130	0.000206	19051.70	0.3	28.26	7.62
1000	0.135	0.000226	18081.70	0.3	26.60	7.80
1200	0.140	0.000247	17987.40	0.3	26.20	8.10
1400	0.150	0.000273	17893.10	0.3	25.70	8.40
1600	0.160	0.000298	15621.95	0.3	19.03	8.70
1800	0.165	0.000324	13350.80	0.3	12.10	9.00
2000	0.170	0.000354	10000.00	0.3	3.70	9.20
2550	0.170	0.000354	200.00	0.3	0.40	9.20

T = Temperature
C_p = Specific heat
λ = Conductivity
E = Elastic Modulus
ν = Poisson's constant
σ_y = Yield stress
α = thermal expansion

Table 2. Temperature dependent material properties for A516-70.

C_p		λ		T	E	ν	σ_y	α
(°F)	(BTU/Lbm-F)	(°F)	(BTU/Sec-inch-F)	(°F)	(ksi)		(ksi)	(10^{-6}/°F)
70	0.11	32	0.000694	72	31000.00	0.3	40.76	7.67
122	0.116	212	0.00067	300	29849.24	0.3	32.98	7.67
302	0.124	392	0.000647	550	28297.79	0.3	32.00	7.67
392	0.127	572	0.000617	700	26991.11	0.3	31.50	7.67
482	0.133	752	0.000571	932	25500.00	0.3	30.10	8.33
572	0.137	932	0.000527	1112	24300.00	0.3	23.70	8.33
662	0.143	1112	0.000476	1292	21000.00	0.3	15.90	8.61
842	0.158	1292	0.000425	1472	17000.00	0.3	8.00	8.61
1022	0.179	1472	0.000348	2732	203.00	0.3	0.44	8.89
1202	0.202	1832	0.000364					
1292	0.342	2192	0.000397					
1382	0.227							
1562	0.215							
1832	0.202							
2192	0.201							

T = Temperature
C_p = Specific heat
λ = Conductivity
E = Elastic Modulus
ν = Poisson's constant
σ_y = Yield stress
α = thermal expansion

Table 3 Temperature dependent material properties for A508 Class 3

C_p		λ		T	E	ν	σ_y	α
(°F)	(BTU/Lbm-F)	(°F)	(BTU/Sec-inch-F)	(°F)	(ksi)		(ksi)	(10^{-6}/°F)
70	0.11	32	0.000694	71.60	30784.93	0.3	54.52	7.67
122	0.116	212	0.00067	600.00	28807.05	0.3	43.78	7.67
302	0.124	392	0.000647	1000.00	25633.87	0.3	29.55	8.33
392	0.127	572	0.000617	1400.00	14540.00	0.3	9.78	8.61
482	0.133	752	0.000571	1800.00	10243.06	0.3	2.78	8.89
572	0.137	932	0.000527	2732.00	203.00	0.3	0.44	8.89
662	0.143	1112	0.000476					
842	0.158	1292	0.000425					
1022	0.179	1472	0.000348					
1202	0.202	1832	0.000364					
1292	0.342	2192	0.000397					
1382	0.227							
1562	0.215							
1832	0.202							
2192	0.201							

T = Temperature
C_p = Specific heat
λ = Conductivity
E = Elastic Modulus
ν = Poisson's constant
σ_y = Yield stress
α = thermal expansion

Table 4 Temperature dependent material properties for S316 and S309

C_p		λ		T	E	ν	σ_y	α
(°F)	(BTU/Lbm-F)	(°F)	(BTU/Sec-inch-F)	(°F)	(ksi)		(ksi)	(10^{-6}/°F)
74.2	0.1079	70	0.000173	75	28400.00	0.30	38.00	8.09
165.4	0.1132	200	0.000186	300	27500.00	0.30	30.00	8.77
191.1	0.1143	400	0.000207	550	25950.00	0.30	23.40	9.33
399.6	0.1229	623	0.000231	700	24900.00	0.30	23.00	9.57
602.6	0.1291	800	0.000248	900	23500.00	0.30	22.00	9.84
794.4	0.132	1011	0.000269	1100	22200.00	0.30	20.50	10.09
1020.5	0.136	1195	0.000288	1300	20820.00	0.30	20.00	10.21
1203.7	0.1398	1391	0.000308	1500	19100.00	0.30	17.00	10.43
1409.6	0.145	1583	0.000327	1652	16900.00	0.30	14.10	10.60
1595.5	0.1505	1783	0.000348	1832	14500.00	0.30	8.46	10.70
1784.2	0.1556	1996	0.000369	2012	14500.00	0.30	3.77	10.90
1995.8	0.1622			2732	203.04	0.30	0.44	11.20

T = Temperature
C_p = Specific heat
λ = Conductivity
E = Elastic Modulus
ν = Poisson's constant
σ_y = Yield stress
α = thermal expansion

Table 5 Temperature dependent material properties for S304

C_p		λ		T	E	ν	σ_y	α
(°F)	(BTU/Lbm-F)	(°F)	(BTU/Sec-inch-F)	(°F)	(ksi)		(ksi)	(10^{-6}/°F)
74.2	0.1079	70	0.000173	75	28400.00	0.30	36.90	8.09
165.4	0.1132	200	0.000186	300	27500.00	0.30	27.70	8.77
191.1	0.1143	400	0.000207	550	25950.00	0.30	23.25	9.33
399.6	0.1229	623	0.000231	700	24900.00	0.30	21.80	9.57
602.6	0.1291	800	0.000248	900	23500.00	0.30	19.90	9.84
794.4	0.132	1011	0.000269	1100	22200.00	0.30	18.10	10.09
1020.5	0.136	1195	0.000288	1300	20820.00	0.30	16.20	10.21
1203.7	0.1398	1391	0.000308	1500	19100.00	0.30	11.40	10.43
1409.6	0.145	1583	0.000327	1652	16900.00	0.30	10.10	10.60
1595.5	0.1505	1783	0.000348	1832	14500.00	0.30	8.46	10.70
1784.2	0.1556	1996	0.000369	2012	14500.00	0.30	3.77	10.90
1995.8	0.1622			2732	203.04	0.30	0.44	11.20

T = Temperature
C_p = Specific heat
λ = Conductivity
E = Elastic Modulus
ν = Poisson's constant
σ_y = Yield stress
α = thermal expansion

Table 6 Temperature dependent creep constants for all the materials

A_s	n_s	T
MATERIAL: A508 Class 2		
1.0000E-26	4.0000	70
2.2910E-12	6.0451	1000
3.2670E-07	4.8865	1200
3.2670E-07	4.8865	2500
Material: A516-70		
1.0000E-26	4.0000	70
2.5060E-13	6.3261	900
1.9920E-09	4.4071	1000
6.9010E-08	4.5039	1100
6.9010E-08	4.5039	2500
MATERIAL: S309, S304, S316		
1.0000E-26	4.0000	70
9.2650E-25	9.7800	887
4.6900E-24	9.9700	932
1.6410E-21	9.0600	977
3.9710E-19	8.2000	1022
2.7540E-18	8.2000	1067
1.7060E-17	8.2000	1112
1.1700E-16	8.1800	1157
7.2180E-16	8.1600	1202
3.4110E-14	7.4200	1247
1.3300E-12	6.7200	1292
2.0930E-11	6.2500	1337
3.2310E-10	5.7700	1382
MATERIAL: INCO182		
1.0000E-26	4.0000	70
1.0000E-26	4.0000	990
2.1478E-16	6.1709	1000
4.6025E-15	6.6426	1100
4.6025E-15	6.6426	2500

$$\dot{\varepsilon}^{s} = \mathrm{A_s}\sigma^{n_s}$$

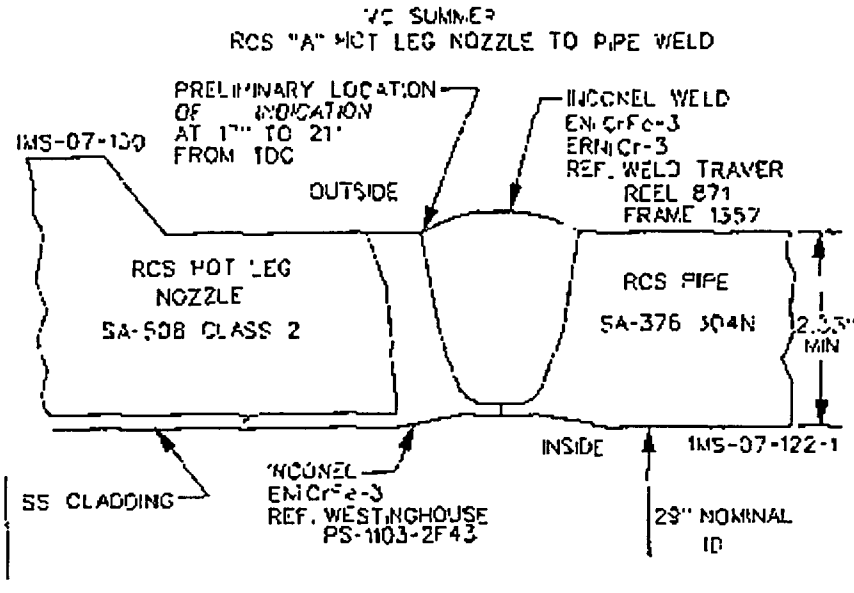

Figure 1. Geometry of VC Summer Hot Leg/RPV Nozzle bimetallic weld joint.

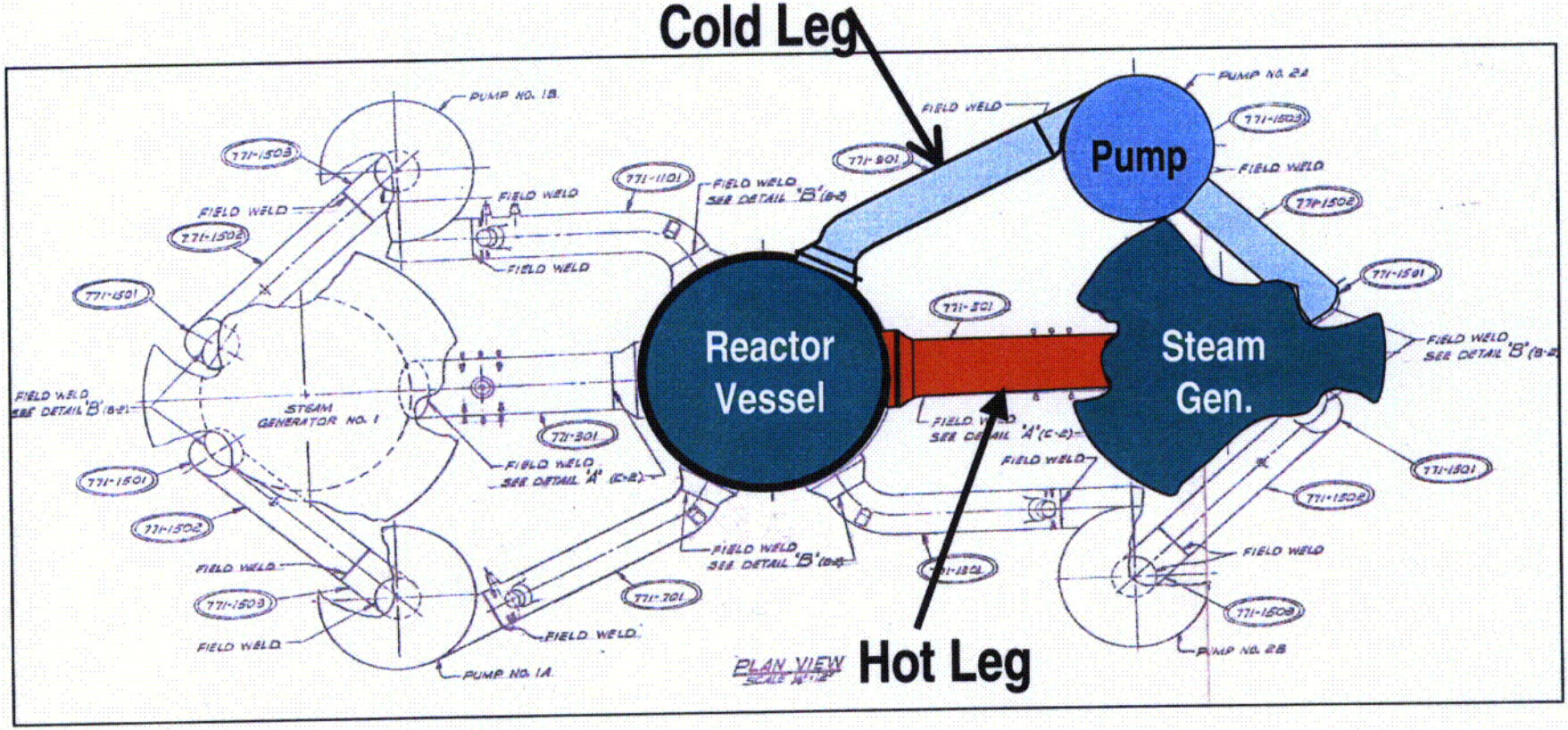

Figure 2. Piping System Geometry.

C05

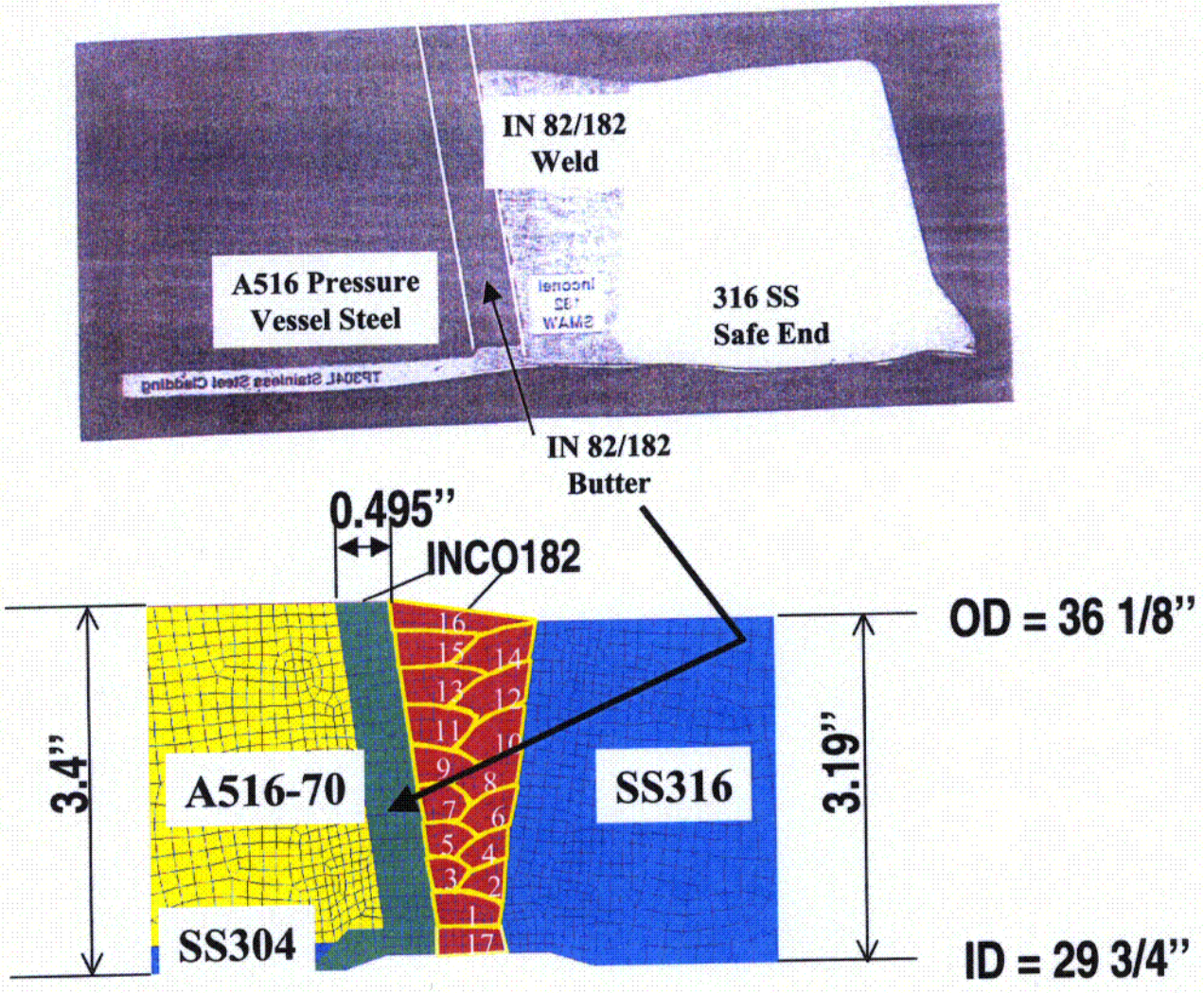

Figure 3. Photo of Cold Leg Weld Cross Section (top) and Computational Weld Model of Cold Leg.

C06

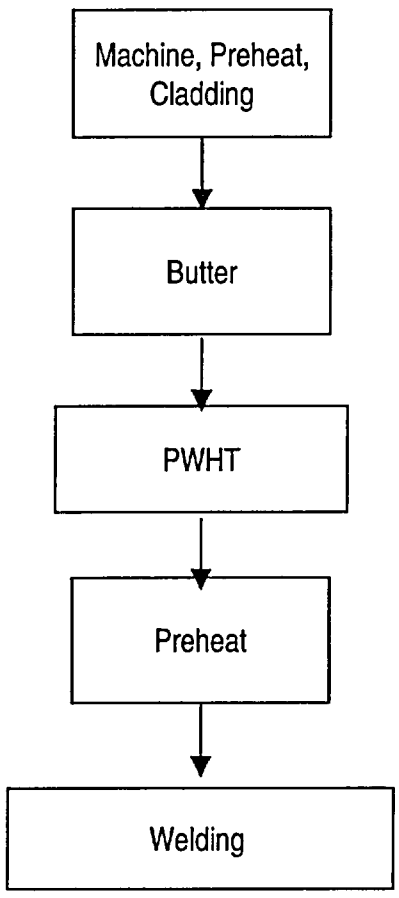

Figure 4. Welding Process Analysis Flow Chart for Cold Leg.

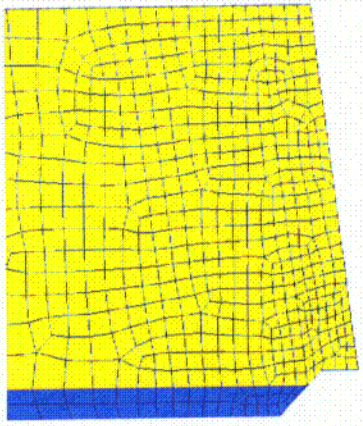

Step 1: Machining

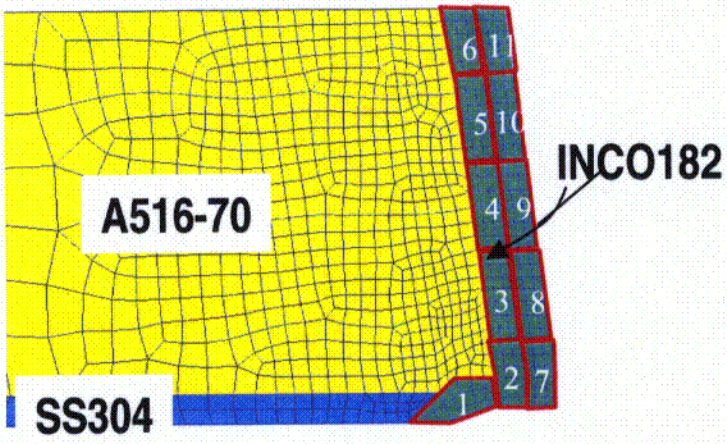

Step 2: Pre-heat, Cladding (304 SS), and Inconel Butter

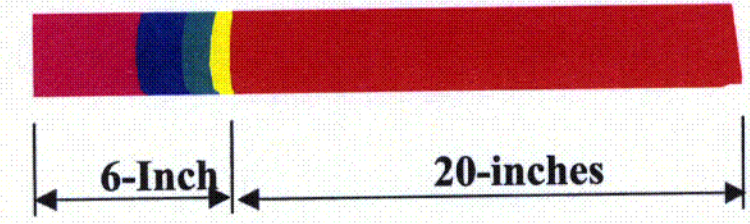

Step 3: Post Weld Heat Treatment (1100F, 4 Hours; 2 Hour Cool Down)

Step 4: Welding to Safe-End

Figure 5. Cold Leg Axis-symmetric Cladding (Buttering) and Weld Model.

C07

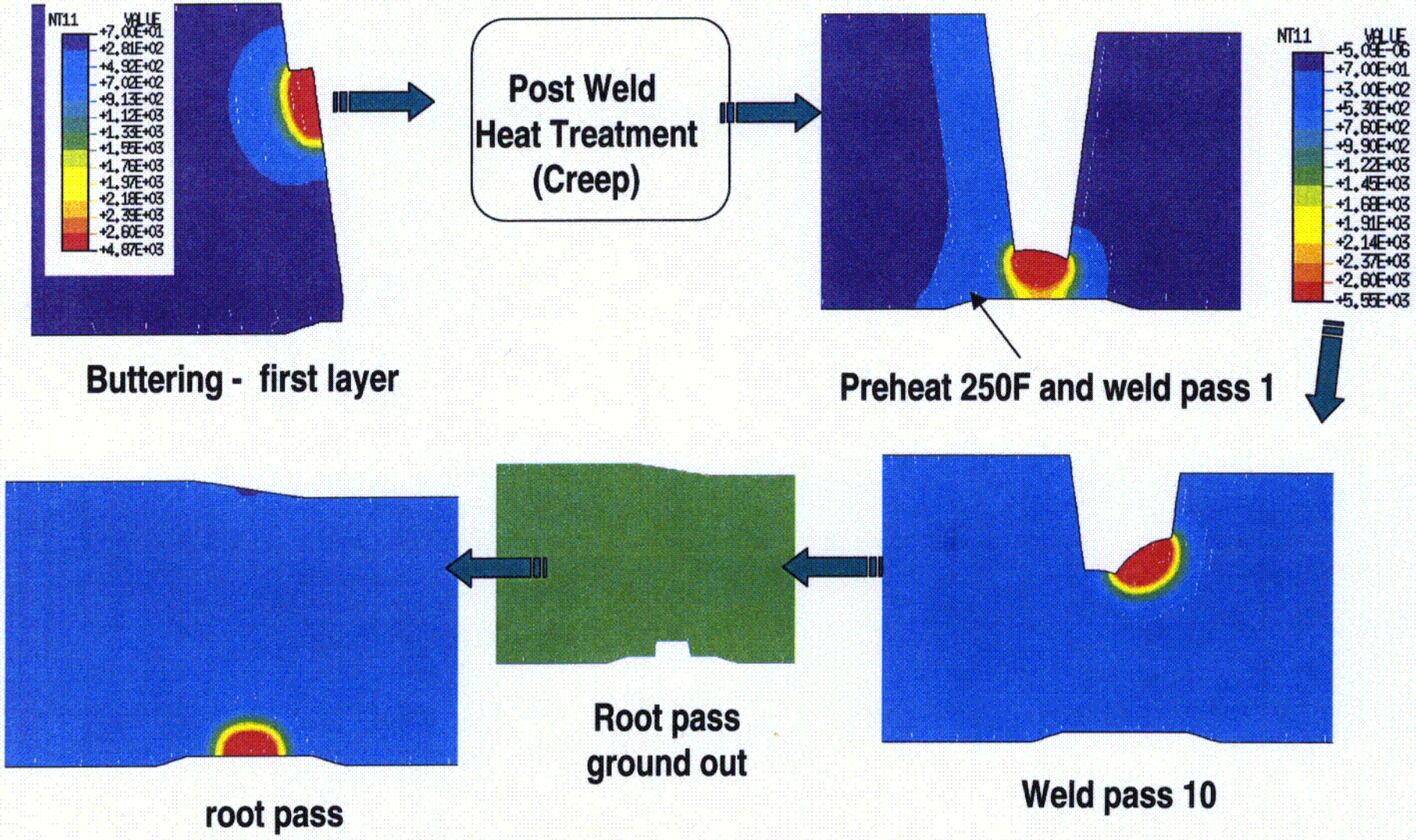

Figure 6. Weld Process Simulation.

C08

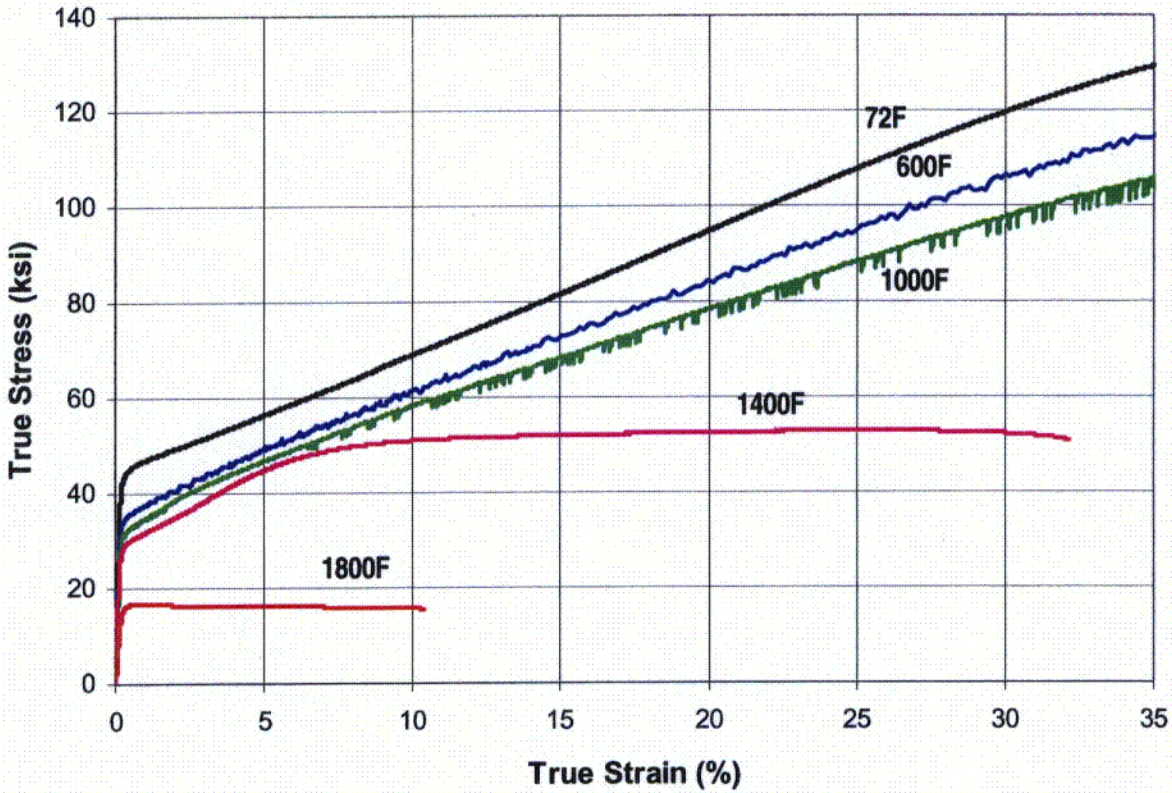

Fig. 7a. Temperature dependent true stress-strain curves of INCO182 tested by ORNL.

C09

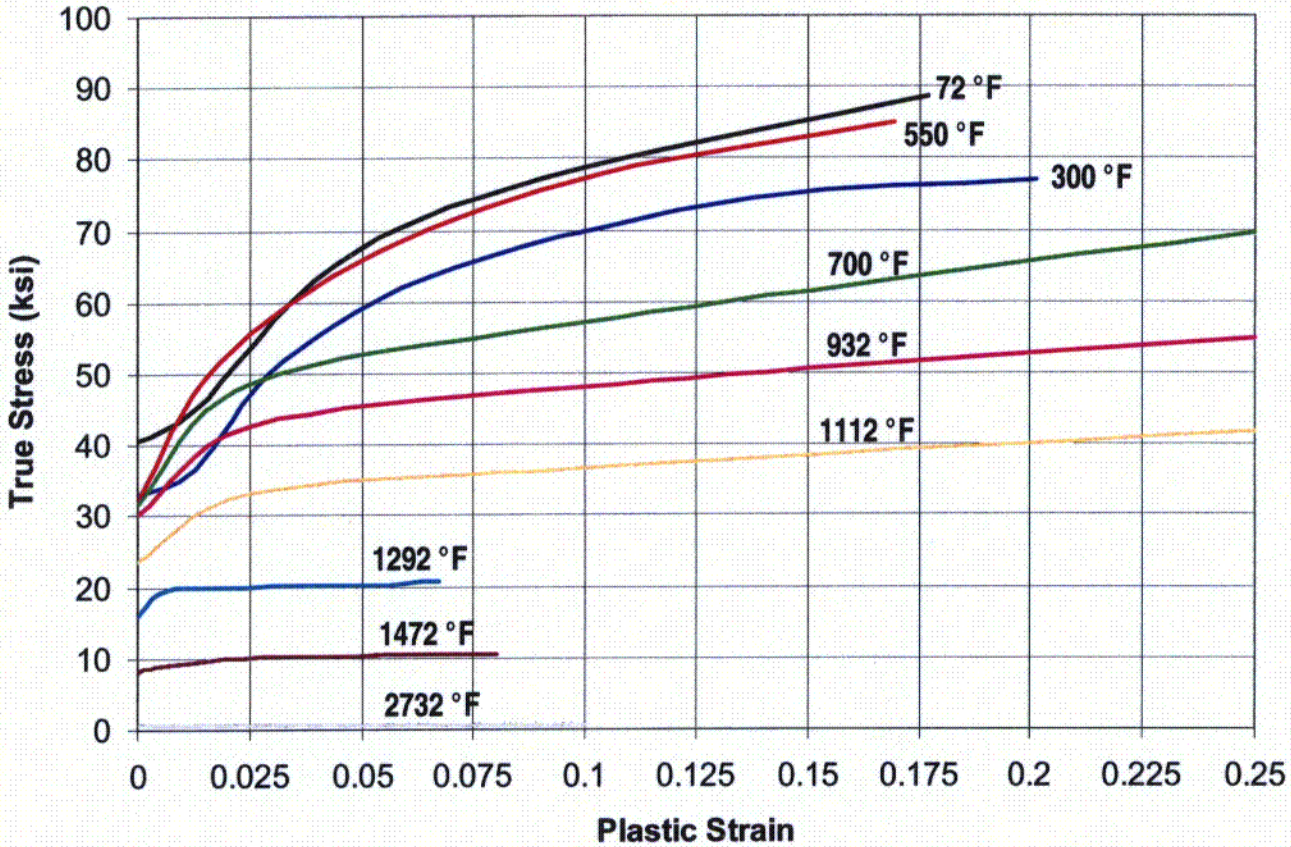

Fig. 7b Temperature dependent true stress-strain curves of A516 Grade 70

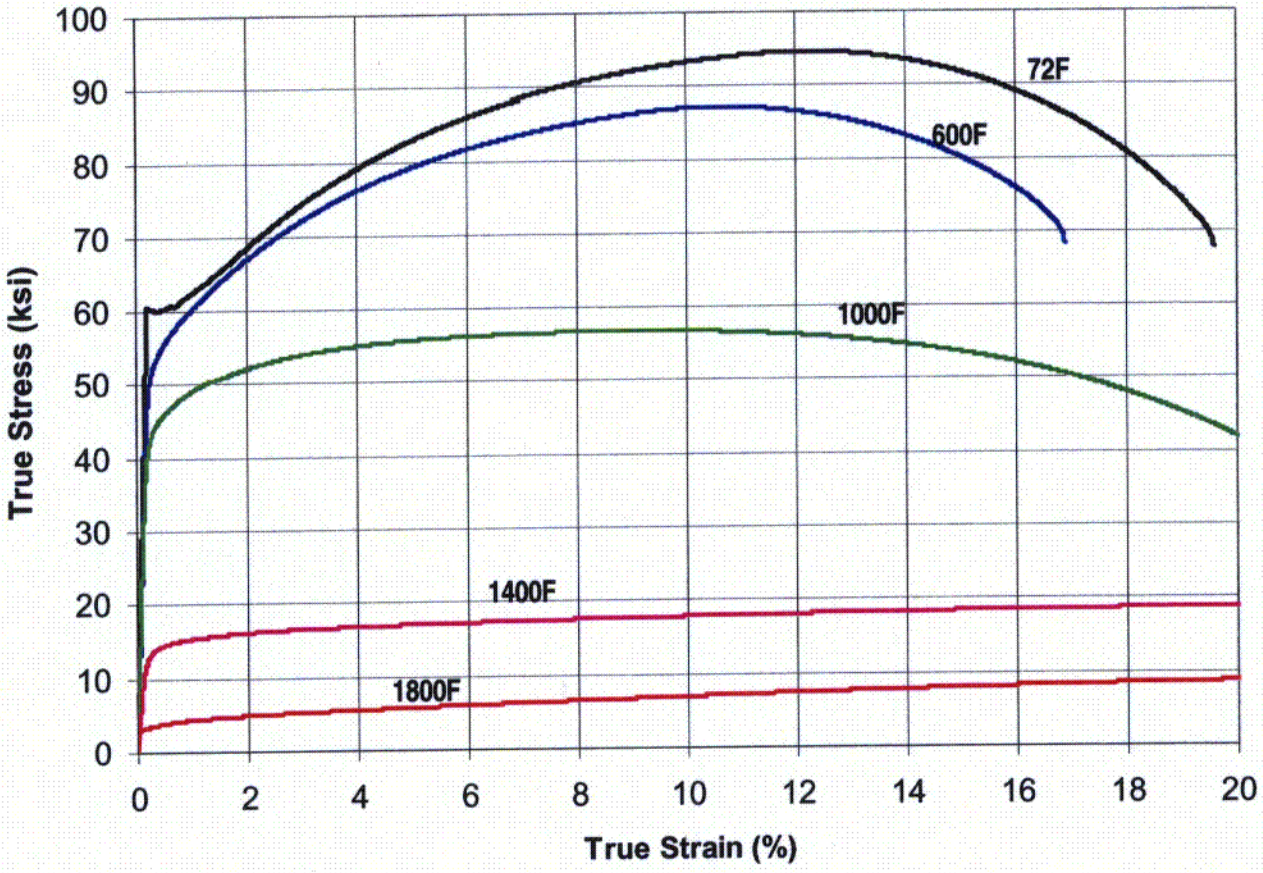

Fig. 7c Temperature dependent true stress-strain curves of A508 Class 3 tested by ORNL

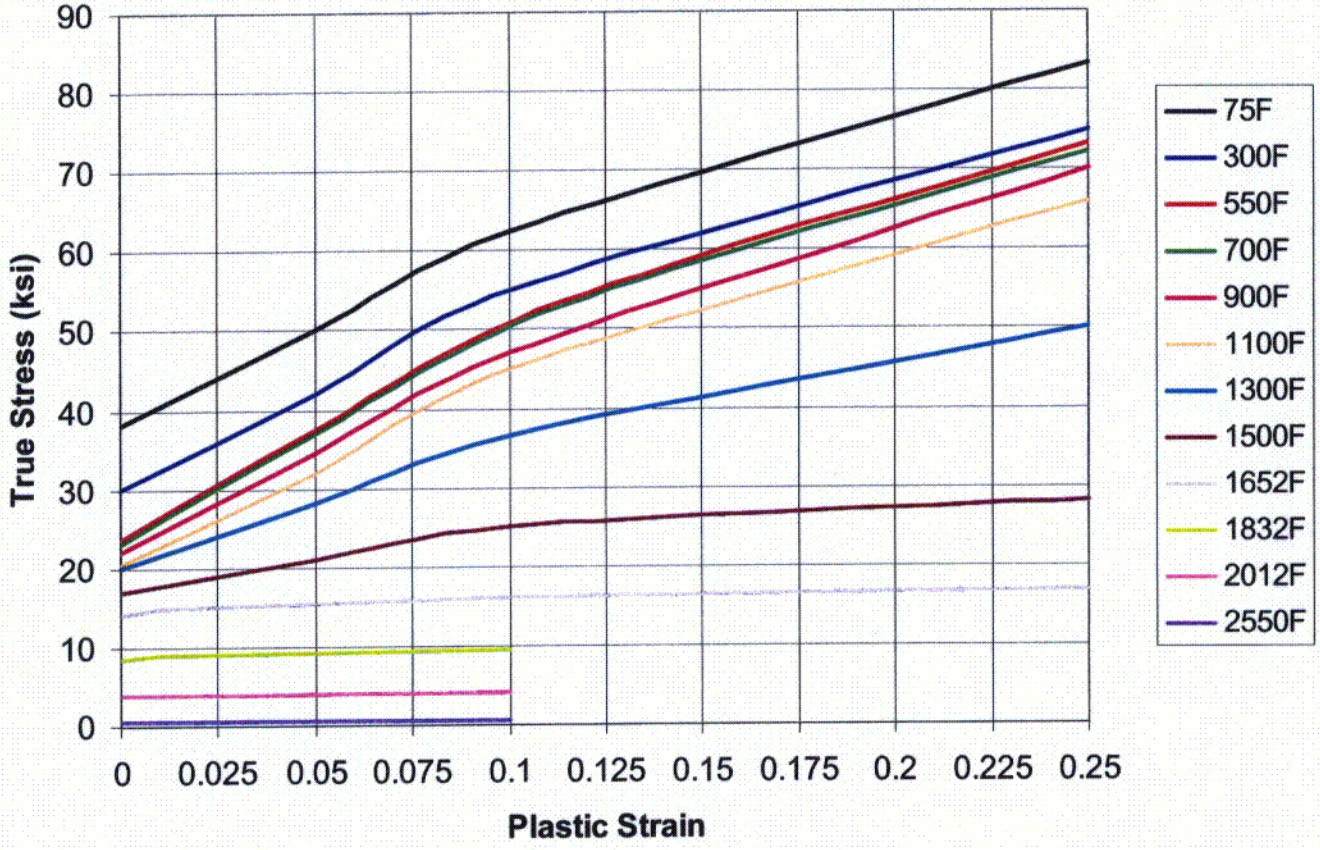

Fig. 7d Temperature dependent true stress-strain curves of S316 and S309

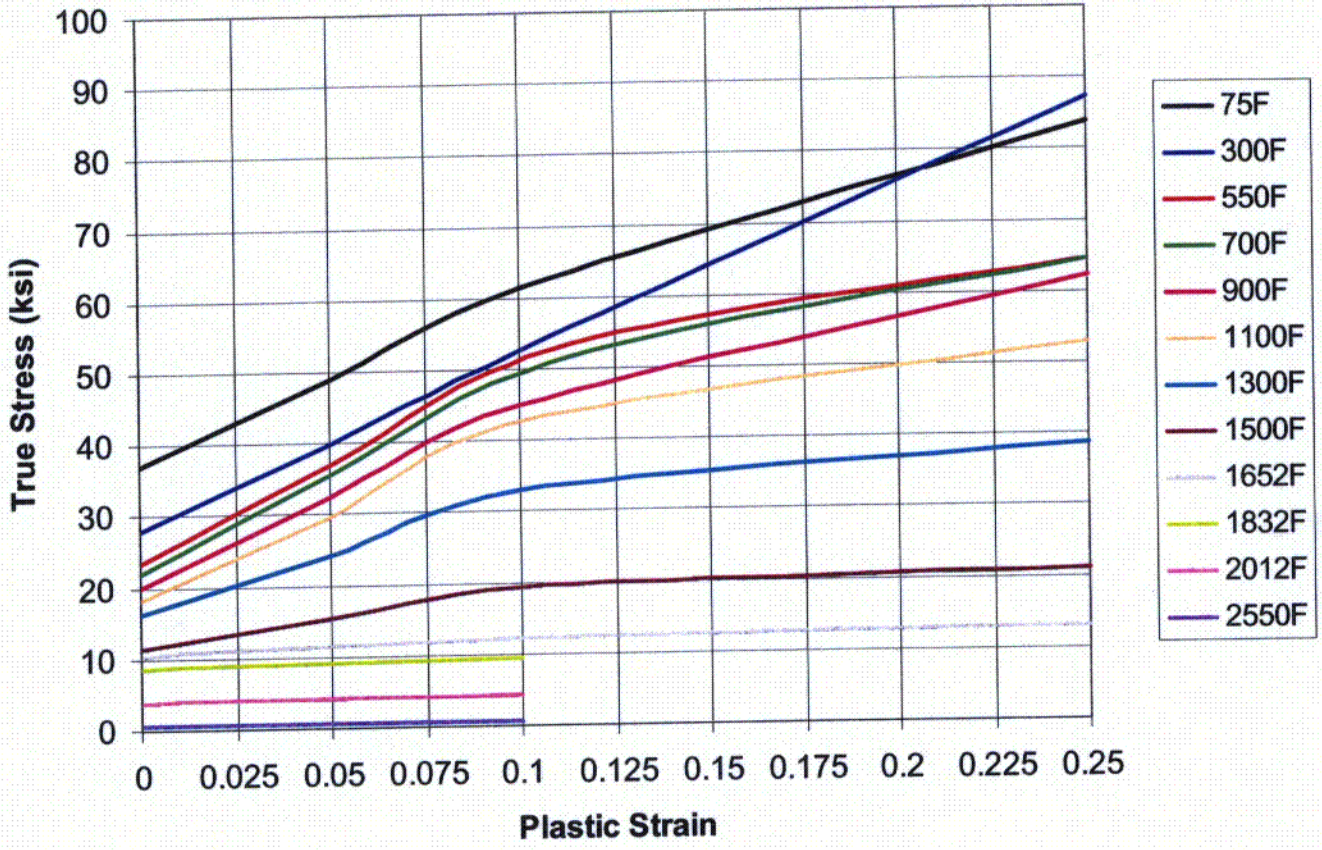

Fig. 7e Temperature dependent true stress-strain curves of S304

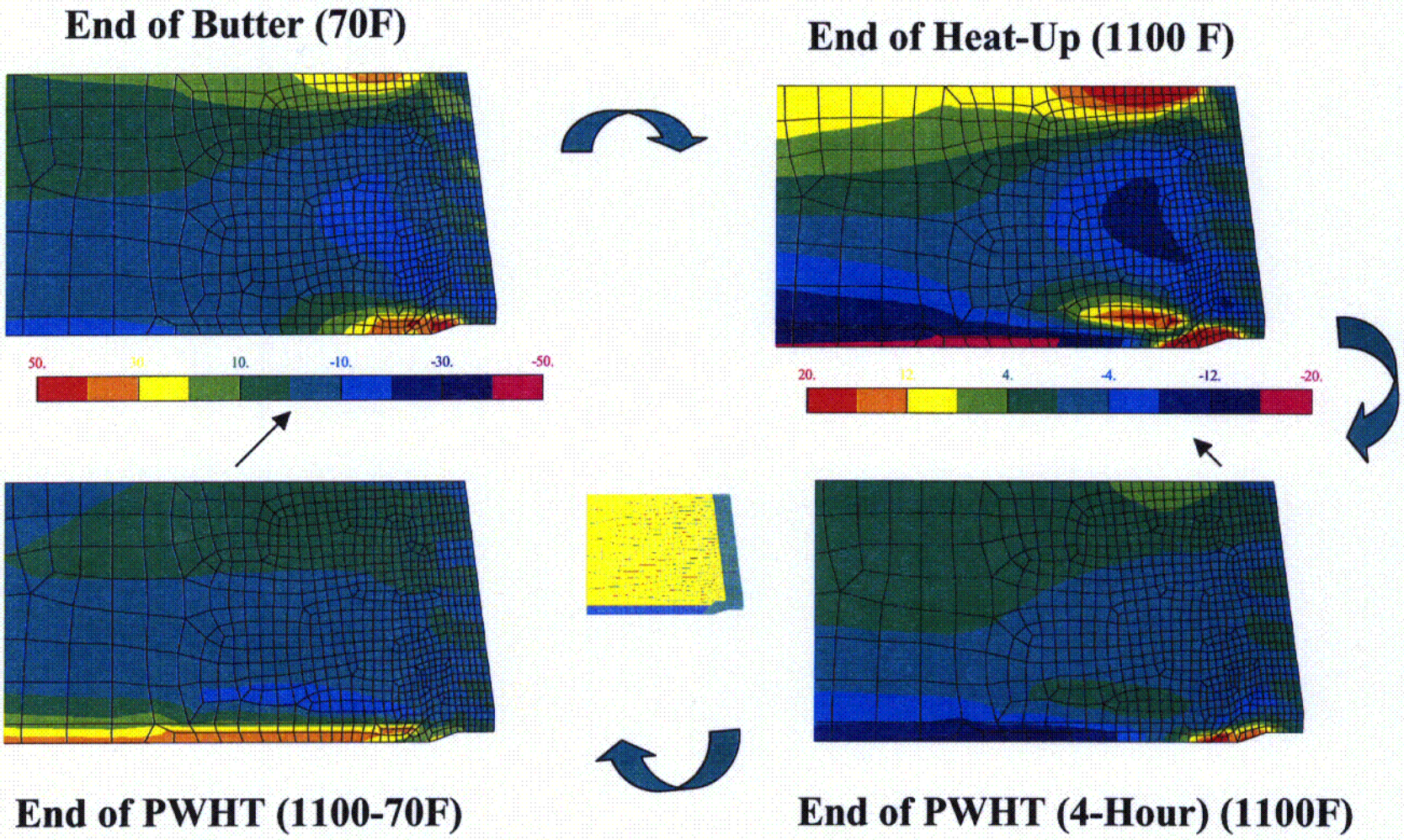

Figure 8. Axial Stresses During Heat Treat Process.

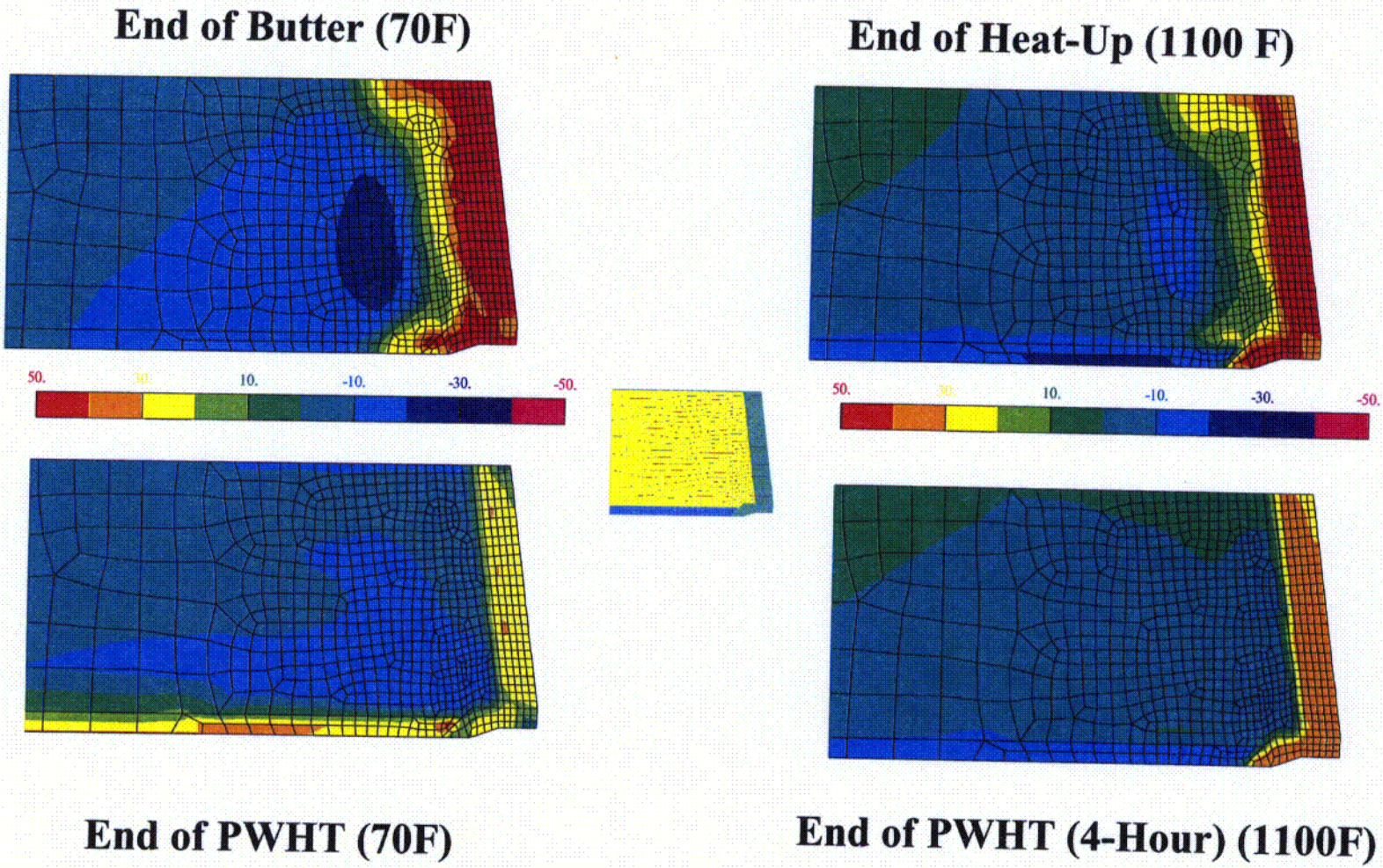

Figure 9. Hoop Stresses During Heat Treat Process.

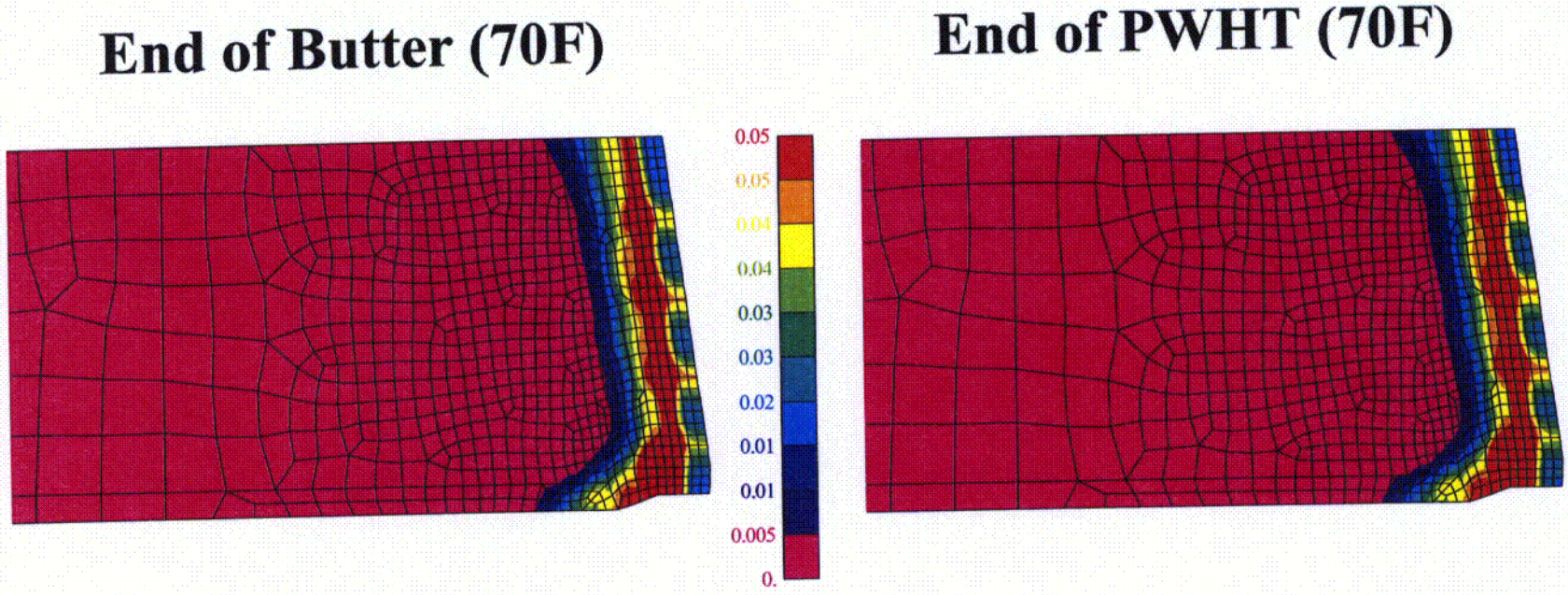

Figure 10. Equivalent Plastic Strains.

End of PWHT (70F)

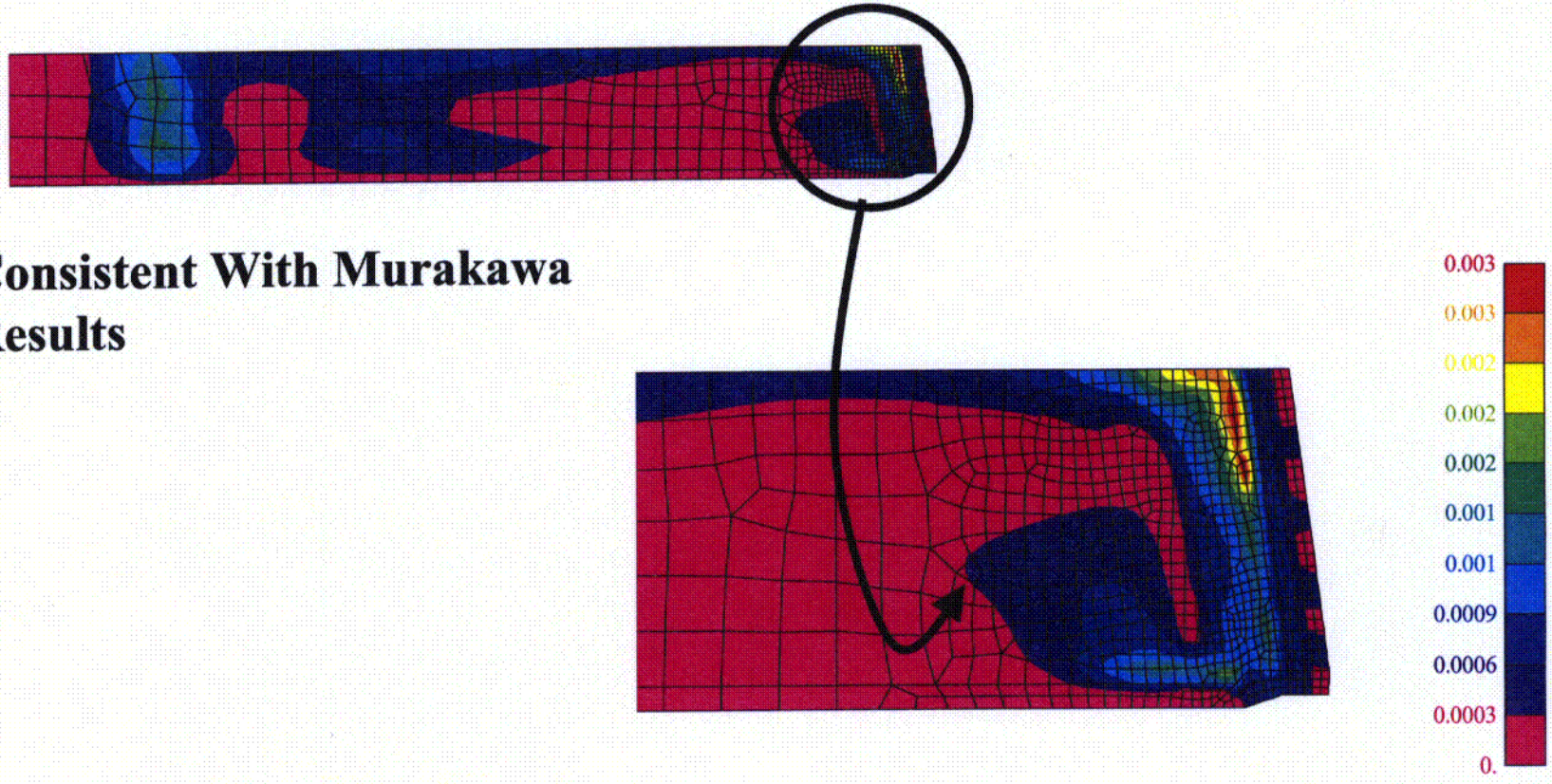

Consistent With Murakawa Results

Figure 11. Equivalent Creep Strains.

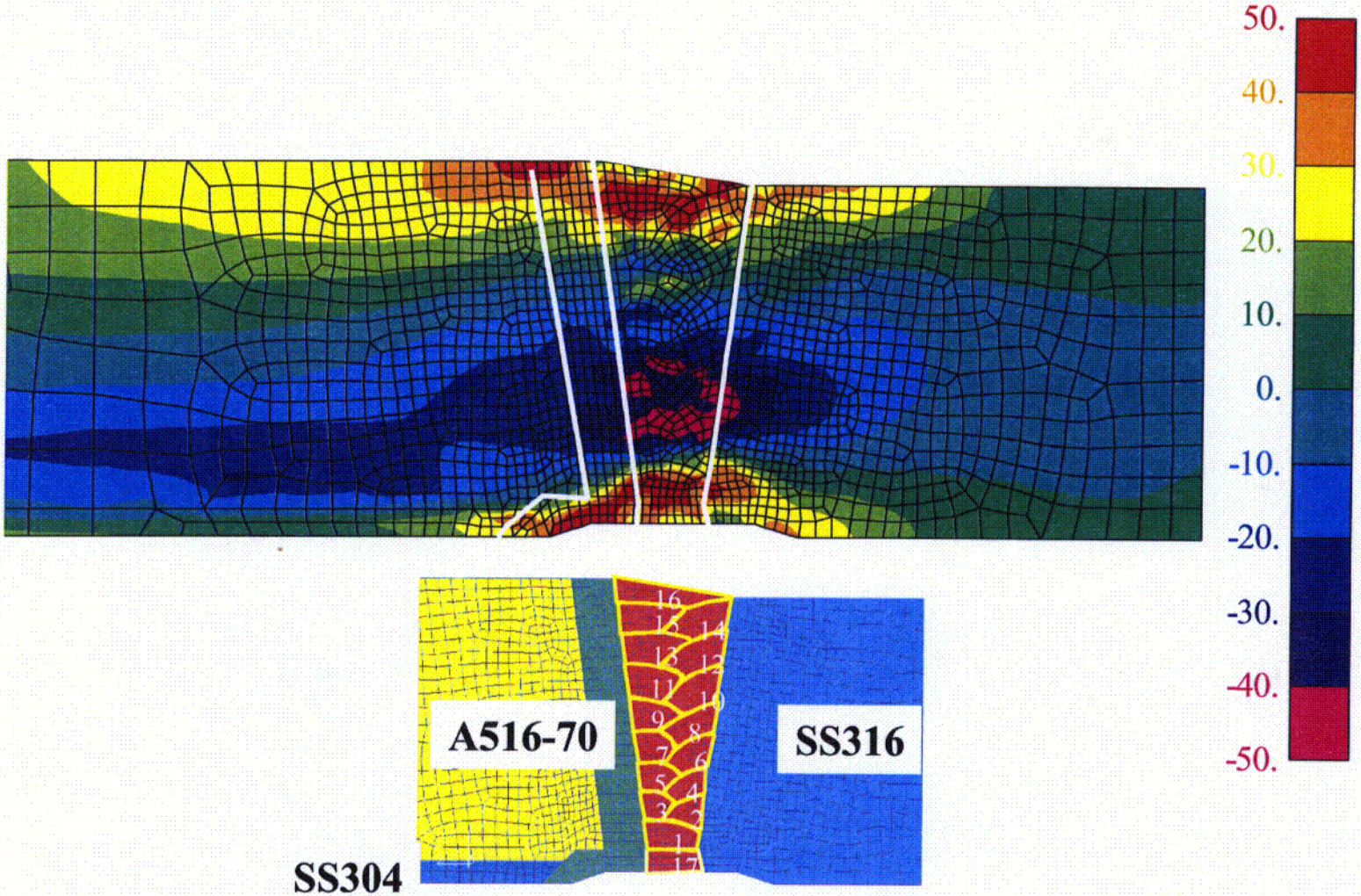

Figure 12. Residual Stresses Final (Axial) at Room Temperature (70 F).

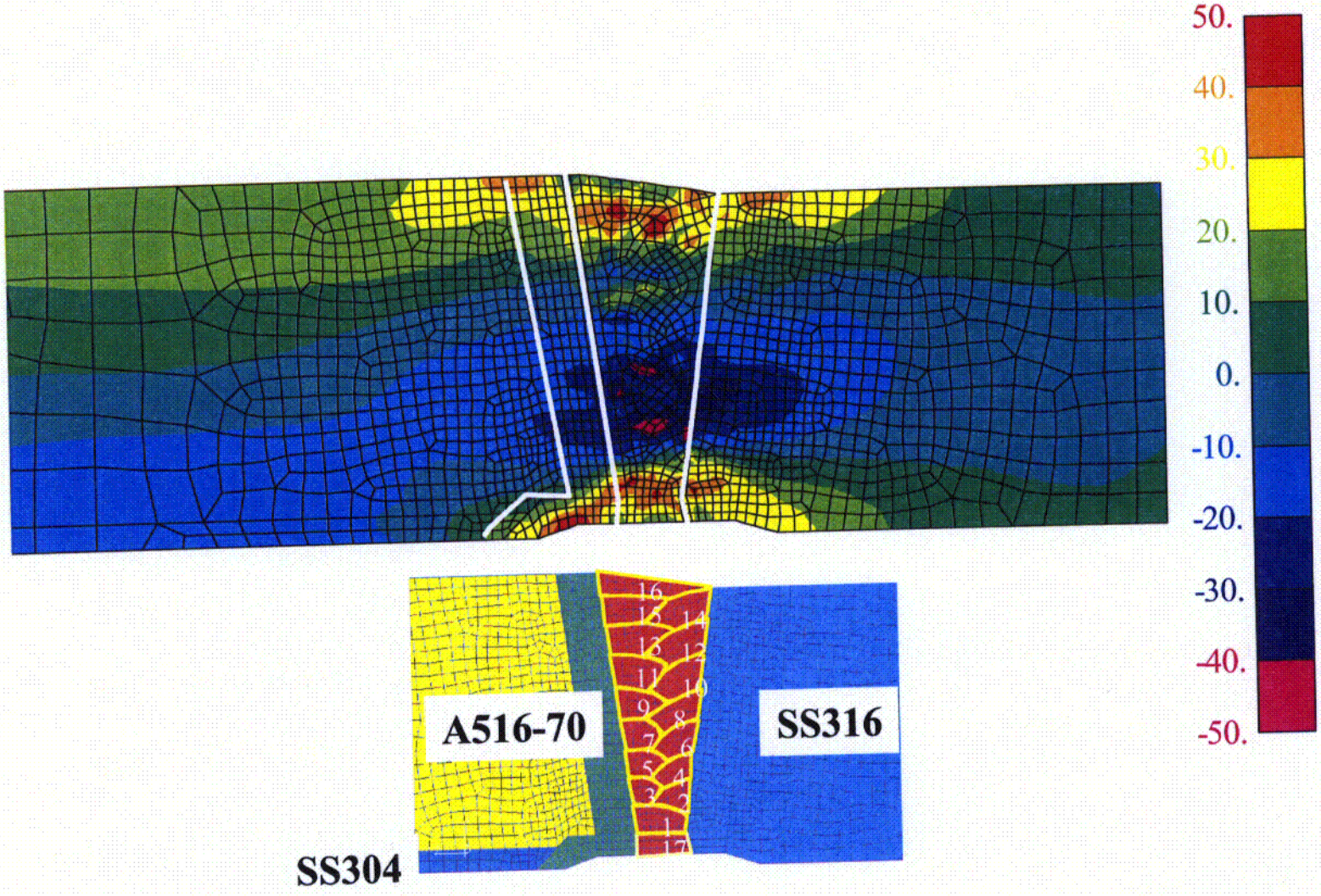

Figure 13. Residual Stresses Final (Axial) at Operating Temperature (556 F).

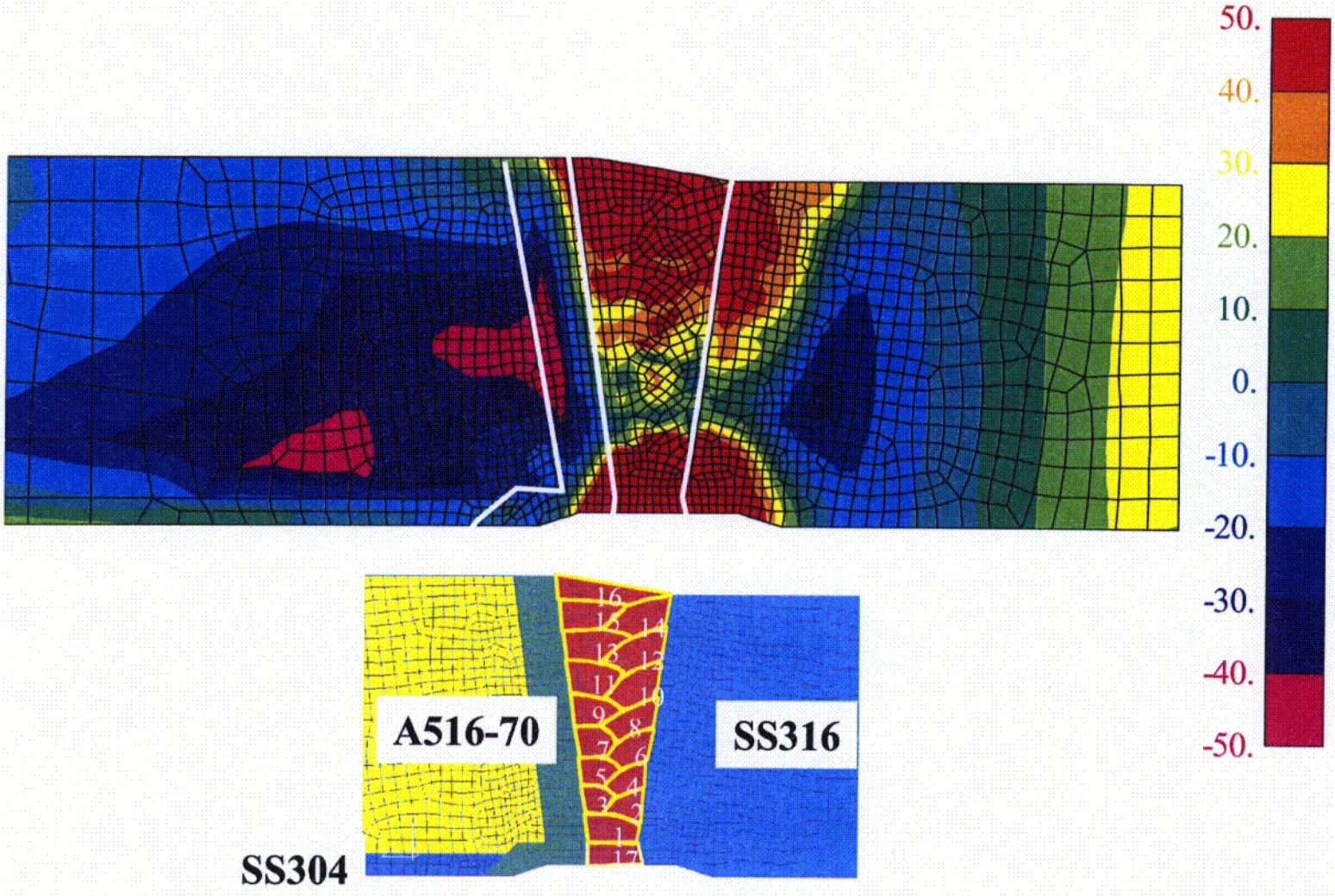

Figure 14. Residual Stresses Final (Hoop) at Room Temperature (70 F).

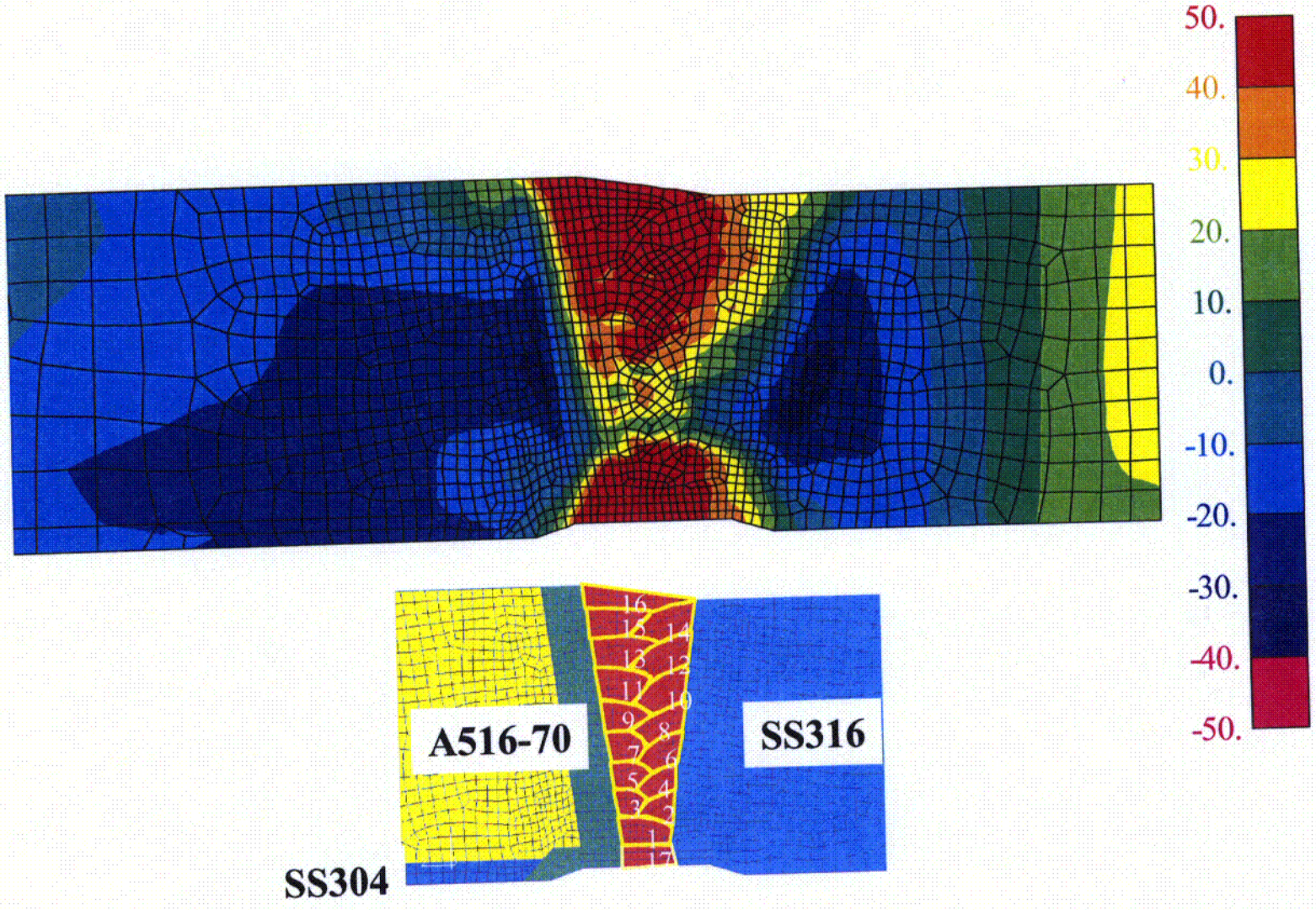

Figure 15. Residual Stresses Final (Hoop) at Operating Temperature (556 F).

Axial Residual Stresses Along OD

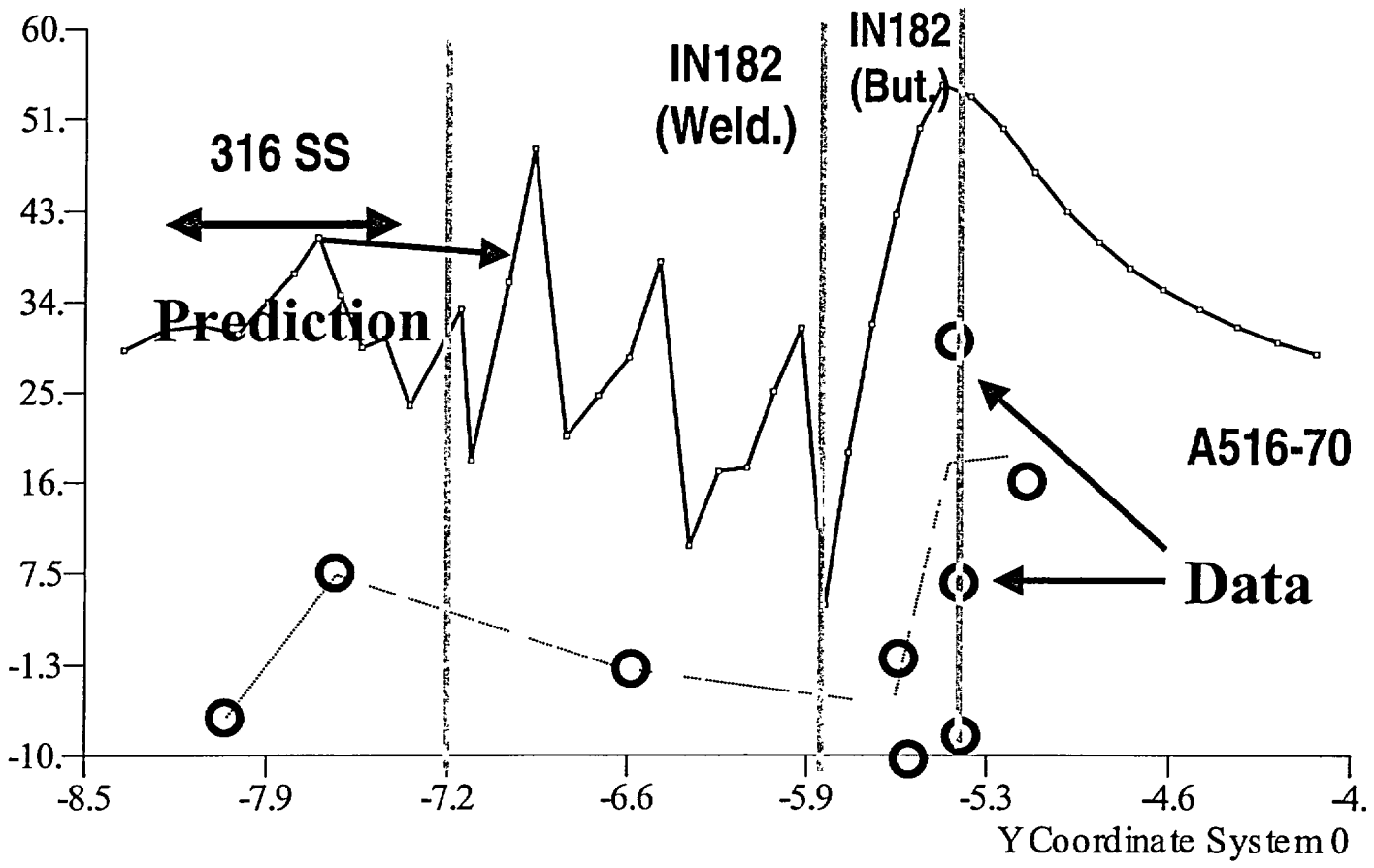

Figure 16 (a). Residual Stresses Final (Hoop) at Operating Temperature (556 F).

Axial Residual Stresses Along ID

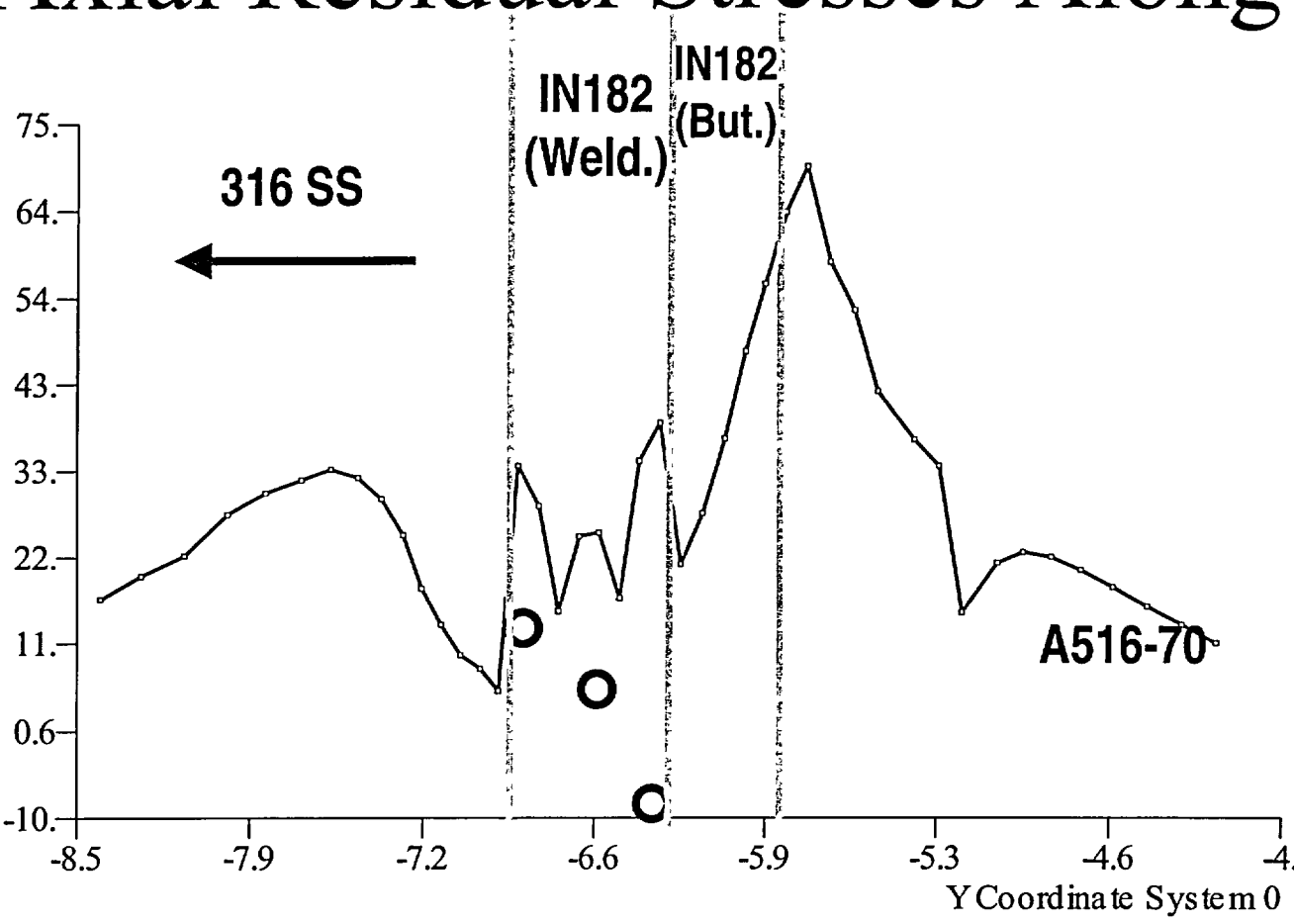

Figure 16 (b). Residual Stresses Final (Hoop) at Operating Temperature (556 F).

Hoop Residual Stresses Along OD

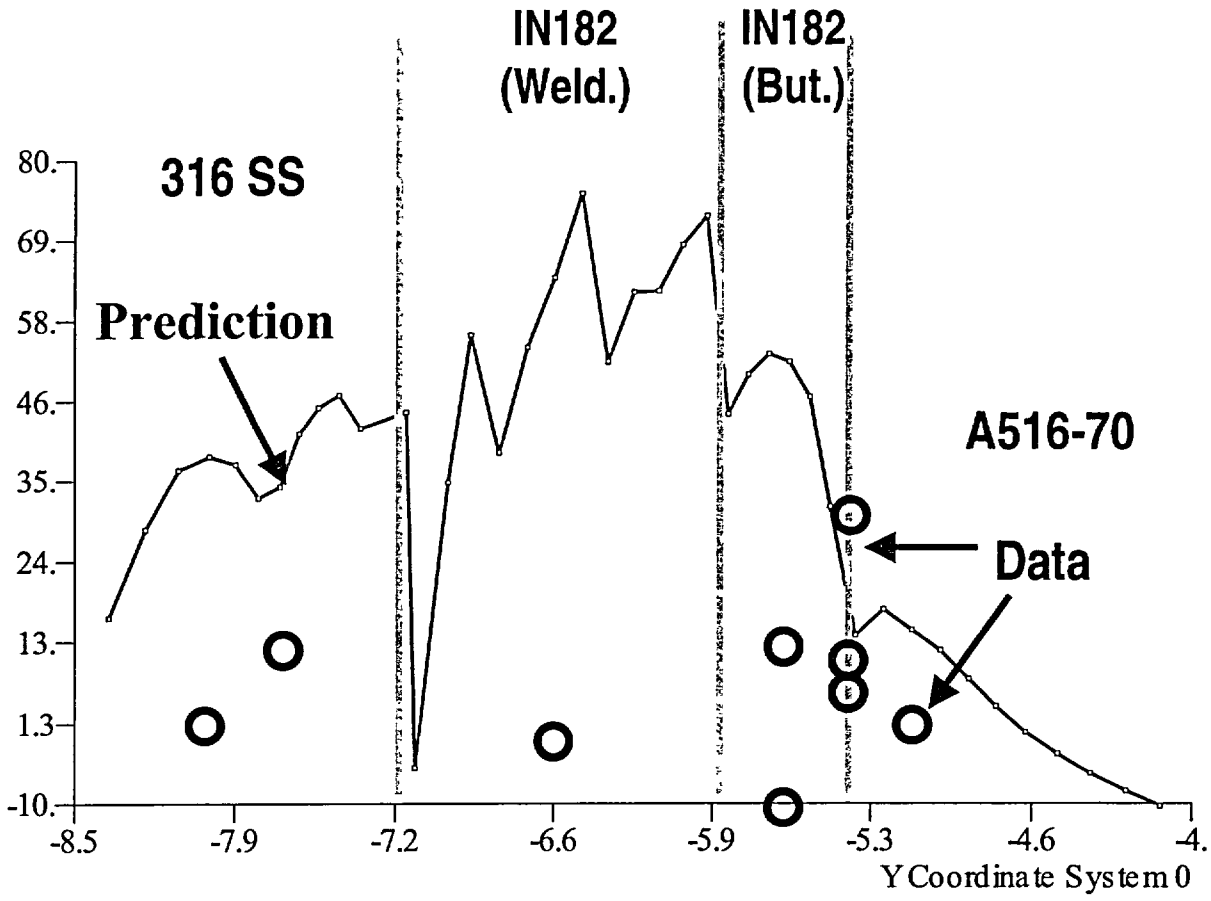

Figure 16 (c). Residual Stresses Final (Hoop) at Operating Temperature (556 F).

Hoop Residual Stresses Along ID

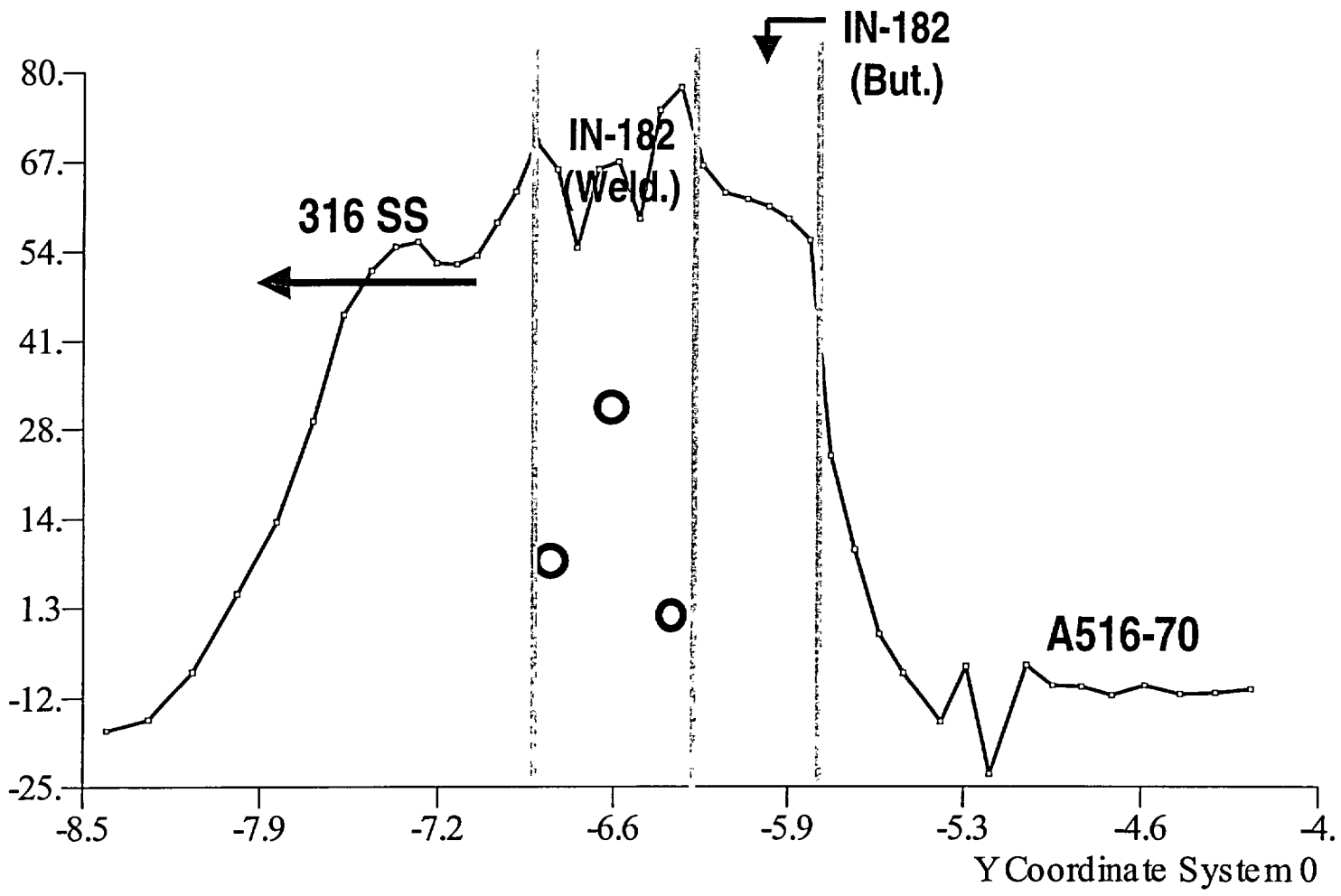

Figure 16 (d). Residual Stresses Final (Hoop) at Operating Temperature (556 F).

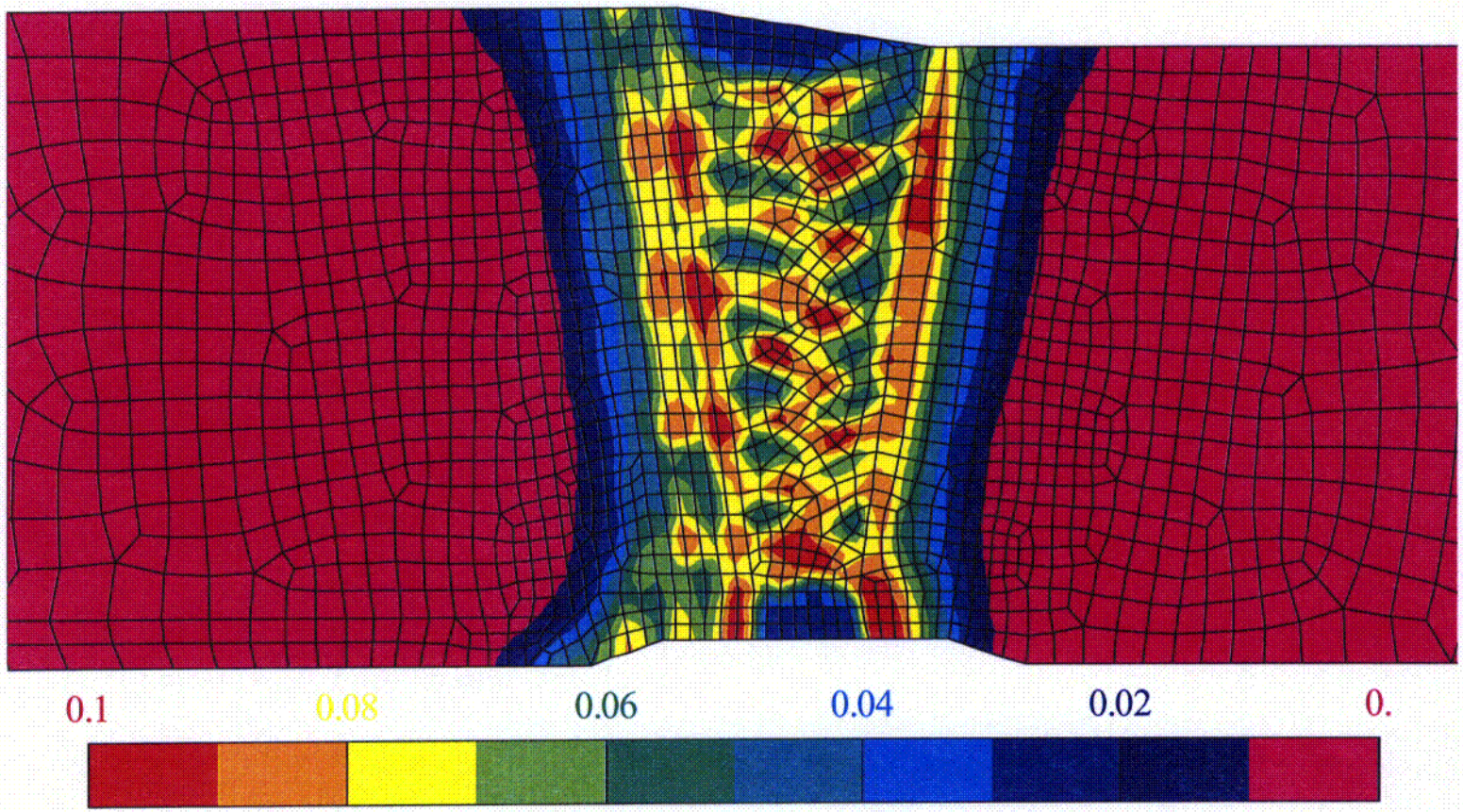

Figure 17. Residual Equivalent Plastic Strains in Cold Leg at Room Temperature.

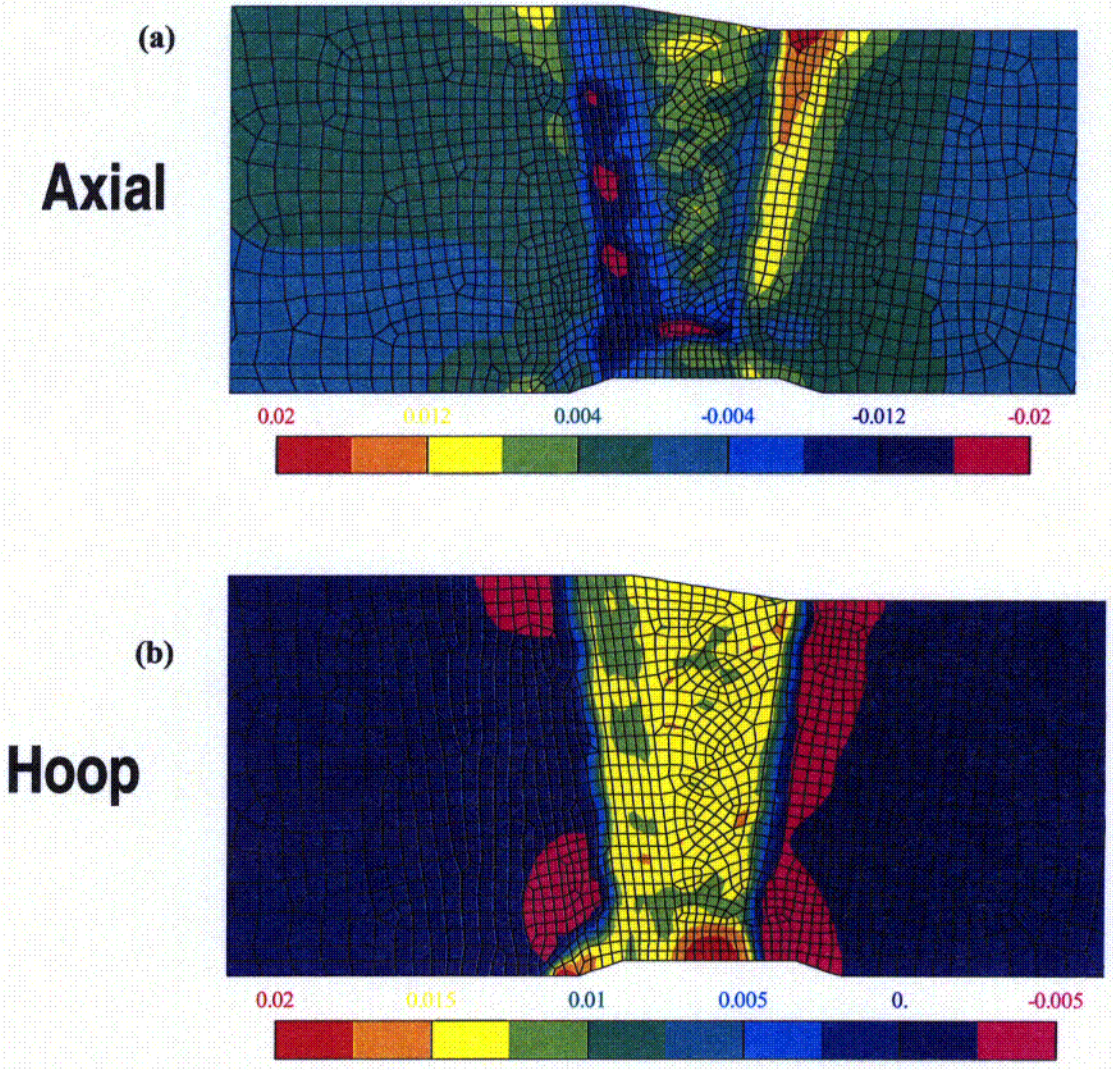

Figure 18. Residual Axial (a), Hoop (b), and Shear (c), Plastic Strains in Cold Leg at Room Temperature.

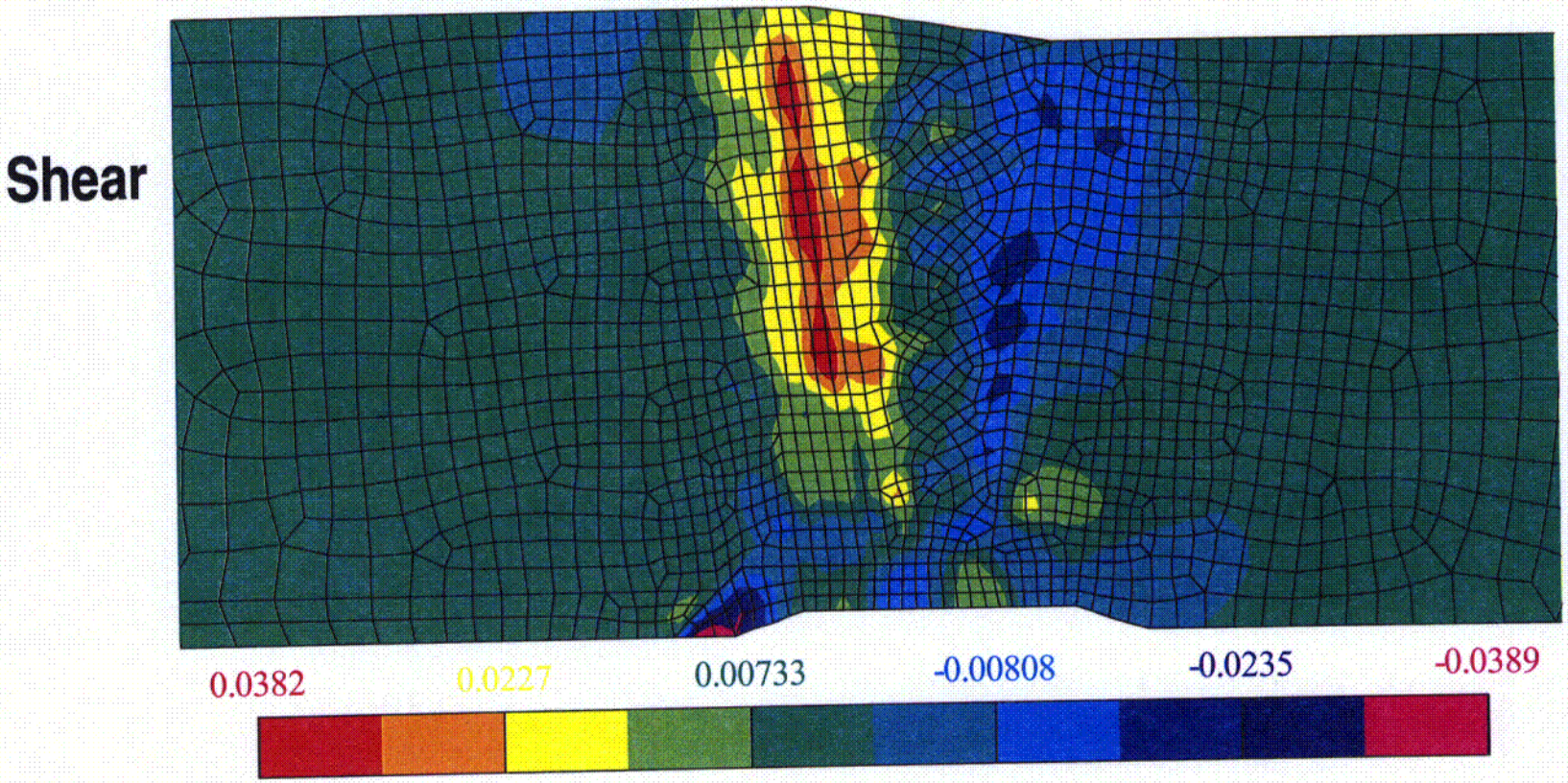

Figure 18. Residual Axial (a), Hoop (b), and Shear (c), Plastic Strains in Cold Leg at Room Temperature.

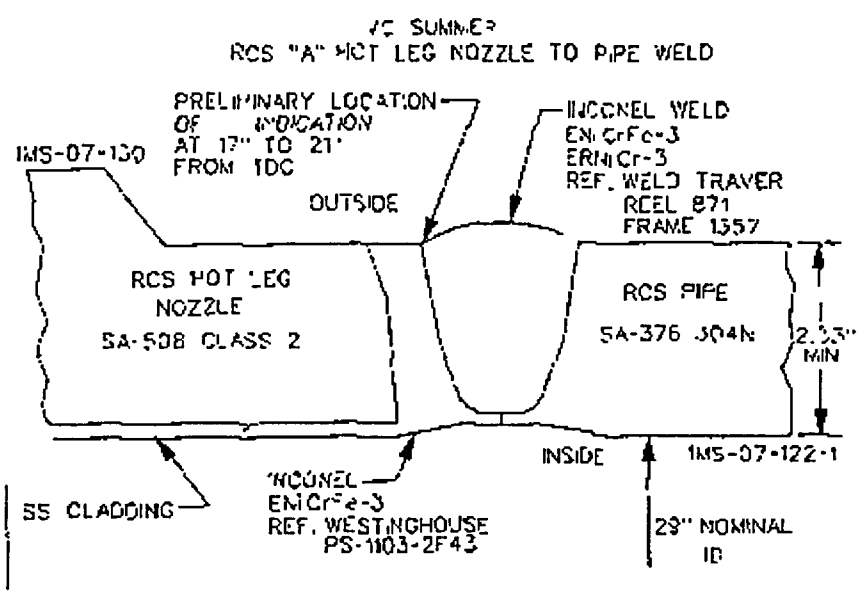

Figure 19. Geometry of VC Summer Bi-metallic weld joint (taken from [1]).

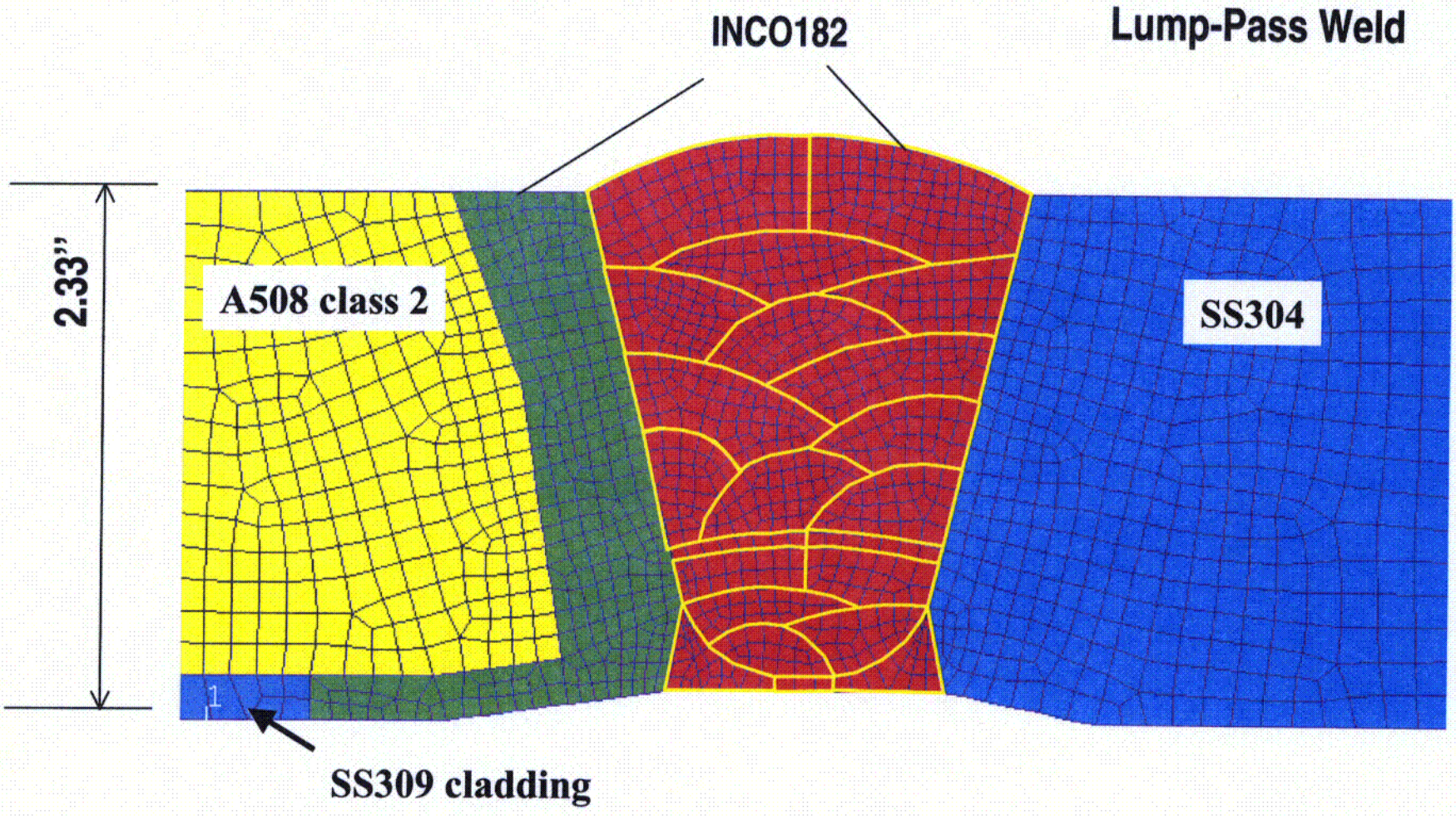

Figure 20. Axis-symmetric Model of VC Summer Bimetallic weld joint.